Transactions of the **14th International Conference on Structural Mechanics in Reactor Technology** (SMiRT 14), Lyon, France, August 17-22, 1997 **CW/2**

# SIERRA : a code to predict the mechanical behavior of LWR fuel rods

**Billaux M.R.(1), Shann S.H.(1), Van Swam L.F.(1), Sontheimer F.(2), Landskron H.(2)**
*(1) Siemens Power Corporation, USA*
*(2) Siemens AG, Germany*

## ABSTRACT

This paper presents the mechanical aspects of the fuel performance code SIERRA. It is shown that the calculation of the cladding deformations of some Super-Ramp rods necessitates an accurate prediction of the gaseous swelling during ramp conditions. The interpretation of ROPE II tests with SIERRA demonstrates that the code gives correct predictions of cladding lift-off. The interpretation of Super-Ramp and HBRP tests shows that there is a correlation between the maximum transient hoop stress in the cladding and the occurrence of cladding failure.

## 1 INTRODUCTION

The SIERRA code (**Si**emens Fuel **R**od Thermal-Mechanical **R**esponse **A**nalysis) has been developed and is currently being further evaluated by Siemens to calculate the behavior of $UO_2$, gadolinia and MOX fuel rods. The model development phase of SIERRA is essentially complete. The majority of the important models of the code have been tested and calibrated either in a stand-alone mode, or in conjunction with other models. This paper deals with the mechanical aspects of the code. Some thermal aspects of SIERRA have been presented in [1].

## 2 CODE STRUCTURE AND MECHANICAL MODELS

SIERRA contains a consistent set of physical models necessary for PWR and BWR fuel performance analysis in normal and off-normal conditions up to cladding failure. The code has a modular structure. It contains a set of stand-alone sub-programs, each of them describing a single physical phenomenon. This enables easy testing of the individual physical models and facilitates the introduction of new or improved models in the future. The subprograms are introduced into a driver program which controls overall progress of the analysis. Special numerical sub-routines have been added to accelerate the convergence of the iterative processes. SIERRA also includes a separate library of material properties.

The main mechanical models are:

- elastic response of the cracked pellet
- fuel densification
- fuel solid fission product swelling
- fuel gaseous swelling
- creep of the pellet
- fuel pellet hourglassing
- elastic response of the cladding
- creep of the cladding
- axial growth of the cladding
- cladding ovalization
- pellet-cladding contact pressure
- axial interaction and trapped stack

Some important features of the mechanical models are presented hereafter.

## 3 MECHANICS OF THE CLADDING

The cladding mechanical model is based on a generalization of the CRASH model [2]. CRASH is a one-dimensional model to simulate the elastic, thermal and creep behavior of the cladding, assuming plane strain and using an axisymmetry approximation. The mechanical model of SIERRA has been generalized to include:

- anisotropic creep of the highly textured cladding
- anisotropic thermal expansion
- temperature dependent anisotropic growth
- effects of waterside corrosion on the mechanics

Elasticity theory is used to calculate the stress and elastic strain distributions in the cladding. The problem consists of solving in each node in the cladding a system of seven equations:

- 3 Hooke's equations
- 3 compatibility equations
- 1 equilibrium equation

Assuming that the elastic modulus and Poisson's ratio are uniform over the cladding thickness, this system has an analytical solution [3]. The integration constants are determined by the boundary conditions: inner and outer pressures, and axial force in the cladding.

## 4 MECHANICS OF THE PELLET

The mechanical model of the pellet also is a one-dimensional model with axisymmetry approximation. In this case, the plane strain approximation is not valid because the pellet stack cannot be properly approximated by a cylinder with infinite length.

The calculation of the stress and elastic strain distributions is accomplished by solving in each radial node of the pellet a system of six equations:

- 3 Hooke's equations
- 2 compatibility equations
- 1 equilibrium equation

The fact that the fuel column is not a solid cylinder but a stack of loose pellets normally with dishes at both ends introduces two-dimensional (r,z) effects. In particular the axial stress at a given radius in the pellet is not uniform along the z-coordinate. This is particularly true close to the dish shoulder. To improve the model predictions, the axial compatibility equation has been replaced with a typical radial distribution of the axial stress at mid-pellet derived from a separate analysis. The axial force in the pellet stack is used as a boundary condition to normalize the axial stress distribution.

An additional hoop strain component has been introduced into the circumferential compatibility equation to simulate the hoop displacements associated with pellet cracking. Moreover, the boundary conditions have been adjusted to take into consideration both pellet cracking and the presence of dishes at both pellet ends. For that purpose, a cracking submodel is employed based on the following assumptions:

- from the very beginning of irradiation, the pellet is cracked into wedge-shaped segments
- the segment pattern is always the most compact possible one: the fragments are in contact with each other along the "bridging annulus"
- at other radial positions, where the radial cracks are open, the hoop stress is equal to the gas inner pressure (with the appropriate sign)
- no additional radial relocation of the fuel is considered

The solution of all necessary equations gives the radial distributions of the stress components in the mid-plane of the pellet. To take into account the two-dimensional effects, the calculation is repeated with an additional thermal expansion component adjusted to give the correct pellet diameter at pellet ends. This provides the pellet-to-cladding contact pressure at the pellet ends and enables the designer to predict the size of the cladding ridges at any time during the irradiation.

The cladding ovality increases with cladding creep down and decreases when the pellet comes into contact with the cladding along the minor axis of the ellipse. To predict cladding ovalization, SIERRA uses a model described by G. Roberts et al. [4]. The program also calculates the local stress at cladding inner surface along the major axis due to cladding bending.

## 5 CALIBRATION AND VALIDATION OF THE ROD MECHANICS

### *5.1 Calibration Data Base*

Calibration of the mechanical models of SIERRA relied on detailed evaluation of rod profilometry, fuel ceramography and cladding metallography, and on the occurrence or not of cladding failure. The individual mechanical models have been calibrated against the following experimental results:

- cladding creep down due to coolant pressure
- outward creep and the formation of ridges resulting from pellet-cladding mechanical interaction
- amount of dish filling
- cladding corrosion thickness
- intragranular and intergranular fuel porosity
- occurrence of cladding failure.

In steady-state operation, the fuel rod mechanics are relatively simple. The full capabilities of the mechanical models can only be properly gaged by comparison with PIE results of rods irradiated under off-normal conditions. To this end, the results of different Studsvik Ramp programs have been extensively used, as well as the results of the ROPE-II program also conducted by Studsvik Nuclear.

### *5.2 Cladding Deformations in Ramp Conditions*

The Super-Ramp program [5] conducted by Studsvik Energiteknik AB investigated the failure propensity of typical light water reactor test fuel rods when subjected to power ramps, after base irradiation to high burnup. A series of five Siemens PWR rods, referred to as PK2 rods, irradiated in the Obrigheim reactor (KWO) up to a burnup of about 45 MWd/kgU presented large cladding deformations with well formed ridges after transient testing, without any of the rods having failed. The detailed results obtained from these rods constitute an excellent test to assess the fuel rod mechanical models. The behavior of rod PK2/3 is analyzed here.

Rod PK2/3 fuel segment was irradiated for four cycles in KWO up to a burnup of 44.6 MWd/kgU and was then ramped in the R2 Studsvik reactor up to a ramp terminal level of 490 W/cm. The rod profilometries before and after the ramp are shown in Figure 1a. The SIERRA results are presented in Figure 1b. The calculated cladding diameters have been corrected in order to take into account the measured outer corrosion layer (48 μm in the middle of the rod segment), so that Figures 1a and 1b are directly comparable. The analysis of the SIERRA results shows that fuel gaseous swelling contributes significantly to the deformation of the pellet (and cladding) during the test. This is experimentally confirmed by longitudinal ceramographies of three of the five tested rodlets (PK2 series) which show evidence of massive gaseous swelling with complete filling of the dishes. The excellent agreement between the measured and calculated deformations validates the calibration of the gaseous swelling model.

### *5.3 Cladding Lift Off*

The ROPE-I (BWR) [6] and ROPE-II (PWR) [7] programs were conceived to study fuel rod behavior when the gas inner pressure exceeds the coolant pressure. One of the objectives of ROPE-II was to investigate the in-pile behavior of three Siemens PWR fuel rodlets irradiated in the Obrigheim reactor (KWO) up to 45 MWd/kgU. Two of the rods were re-fabricated and overpressurized to a pressure equivalent to 78 and 138 bar above the system pressure at hot in-reactor conditions. The three rodlets were irradiated in the R2 reactor for 114 days under typical PWR conditions. The irradiation was several times interrupted to perform profilometry measurements. The set of profilometry measurements were used to characterize in detail the creep behavior of the cladding in non lift-off and in lift-off conditions. The behavior of rod K1 is analyzed here.

Rod K1 fuel segment was irradiated for four cycles in KWO up to a burnup of 42.6 MWd/kgU. The diametral creep down during base irradiation was in the range 68 to 71 μm. Profilometry performed after base irradiation showed well formed ridges. The oxide layer thickness was in the range of 20 to 30 μm. Fission gas release was below 1%. The K1 rod was transported to Studsvik, and was refabricated and pressurized with a mixture of argon and xenon to simulate the composition of the fission gas. The rod was operated in the R2 reactor at a linear power of 196 W/cm. The rod inner pressure was as high as 280 bar; i.e., 138 bar above the coolant pressure.

Profilometry performed after 3 days of irradiation showed that pellet-cladding interaction (PCI) persisted at the very beginning of the R2 irradiation. Figure 2a presents the pellet-cladding contact pressure and the hoop stress in the cladding calculated by SIERRA. The left part of the graph, up to 1143 days is related to the base irradiation in KWO. The period beyond 1143 days corresponds to the irradiation in the R2 reactor. Onset of PCI occurs between 800 and 900 days: the contact pressure and the hoop stress in the cladding rise. The latter becomes positive (tensile) in the last 200 days of base irradiation. The fluctuations are due to the variations of rod power. In the R2 reactor, the internal rod overpressure of 138 bar combined with a residual contact pressure leads to a high tensile stress level in the cladding and to the total relaxation of the contact pressure within a few days. During that period of time, the hoop stress in the cladding decreases from 125 to 80 MPa. The subsequent creep-out of the cladding, by about 14 μm over the remainder of the irradiation period, is then controlled by the overpressure only. Figure 2b shows the calculated lift-off of the cladding in the R2 reactor together with the profilometry measurements.

### *5.4 Clad Failure Prediction*

Fuel performance code should be capable of predicting the occurrence of rod failure during power ramp conditions. When the reactor has been operated during a prolonged period of time at relatively low power, any significant increase of the local power in a fuel rod may contribute to stress the cladding. The hoop and axial stresses in the cladding may increase rapidly and exceed the stress corrosion cracking (SCC) threshold. Stress corrosion cracking progresses within the cladding under the combined effect of the chemical influence of fission products and of tensile stresses until the cladding fails. Benchmarking of SIERRA showed that in classical ramp tests, there is a relation between the calculated maximum hoop stress at the cladding inner surface at the pellet-to-pellet interface during the ramp and the occurrence of failure. The maximum transient hoop stress generally occurs at the peak of the power ramp and failure takes place a few seconds to some minutes later depending on the stress level.

The SIERRA SCC benchmarking data base includes all the PWR Siemens and Westinghouse rods of the Super-Ramp program [5] with solid pellets, as well as thirteen rods of the High Burnup PWR Ramp Test Program (HBRP) [8]. The HBRP, sponsored by US Department of Energy (DOE), is a program specifically designed for transient testing of PWR fuel. The Siemens fuel rods in this program were base irradiated in KWO and submitted to power ramps in the High Flux Reactor (HFR) at Petten.

Figure 3 indicates that the failure threshold decreases when the hydride orientation factor of the cladding increases. When the latter is larger than 0.15, the failure threshold is close to 415 MPa. This stress level is much higher than the SCC threshold derived from out-of-reactor tests. The main reason is that in the out-of-reactor test, the stress is a steady-state stress; whereas, in the ramp tests it is a transient stress. The latter, after reaching its peak value at the top of the ramp, relaxes very rapidly. The failure threshold was found to be independent of the amount of fission gas released in the free volumes. It seems that in ramp conditions at burnups larger than 10 MWd/kgU, there are always enough harmful fission products in contact with the inner surface of the cladding to induce SCC.

### *5.5 Cladding ovality*

Figure 4 illustrates the evolution of the ovality of rod 1/13 of the HBRP program [5]. Rod 1/13 was irradiated in the KWO reactor to a burnup of 22 MWd/kgU and submitted to a power transient in the HFR to a power of 52 kW/m. Figure 4 shows both the Sierra prediction and the measurement results. The cladding ovality is defined as the difference between the maximum diameter and the minimum diameter at an axial location. The measured ovality is measured in cold conditions. The calculated ovality is the ovality of the free-standing cladding without the elastic deformations due to PCI.

During base irradiation in the KWO reactor, the ovality of rod 1/13 at the level of the power peak increases from the as-fabricated value of 12 μm to about 54 μm. At that time, contact between pellet and cladding is established along the short axis of the ellipse. During the last weeks of irradiation in KWO, the cladding ovality decreases a little as the pressure of the pellet on the cladding increases. In the HFR, the rod was preconditioned during 400 hours at 28 kW/m. This higher power contributed to increase the mechanical interaction between pellet and cladding and to decrease cladding ovality. The power was then rapidly increased up to 52 kW/m and maintained at that level for 13.5 minutes before reactor shutdown. During those 13.5 minutes, the ovality dropped to about 35 μm. The good agreement between the calculation and the measurement results from the proper calibration of the ovalization model of SIERRA.

## 6 CONCLUSIONS

The SIERRA fuel performance code has been developed as a state-of-the art code for modelling the thermal and mechanical behavior of PWR and BWR fuel rods in normal and off-normal conditions. In normal operating conditions, SIERRA has the capability to predict the conditioning and the deconditioning states of fuel rods subjected to varying power levels. In off-normal conditions, the code gives a reliable prediction of the cladding deformations resulting both from pellet-cladding mechanical interaction and from high inner pressure. The risk of cladding failure by stress corrosion cracking due to a fast power increase can also be assessed. These new capabilities will enable fuel rod designers to better use margins with respect to design and safety criteria.

## 7 REFERENCES

1. M. R. Billaux, S.-H. Shann, L. F. Van Swam & F. Sontheimer, "SIERRA: a Fuel Performance Code to Predict the Mechanical Behavior of Fuel Rods up to High Burnup," International Topical Meeting on Light Water Reactor Fuel Performance, Portland, Oregon, March 2-6, 1997.

2. M. Guyette, "CRASH - A Computer Program for the Evaluation of the Creep and Plastic Behavior of Fuel Pin Sheaths," Nucl. Appl. & Techn. 9 (1970) 60-69.

3. M. R. Billaux, S.-H. Shann & L. F. Van Swam, "Transient Fuel Rod Behavior Prediction with RODEX-3/SIERRA," IAEA Technical Committee Meeting on Water Reactor Fuel Element Modelling at High Burnup and its Experimental Support, Windermere, England, September 19-23, 1994.

4. G. Roberts & K. W. Jones, "Axial Gap Formation in PWR Fuel Pins," CEGB RD/B/N4321, July 1978.

5. H. Mogard & H. Heckermann, "The International Super-Ramp Project at Studsvik," Light Water Reactor Fuel Performance, Orlando, Florida, April 21-24, 1985, p. 6-17, American Nuclear Society, La Grange Park, Illinois (1985).

6. D. Schrire, F. Sontheimer & G. Lysell, "ROPE-I, The Studsvik BWR Rod Overpressure Experiment," International Topical Meeting on LWR Fuel Performance, West Palm Beach, Florida, April 16-19, 1994, p. 212, American Nuclear Society, La Grange Park, Illinois (1994).

7. F. Sontheimer & M. R. Billaux, "Mechanical Analysis of the Siemens Rods During ROPE-II Start-Up with a New Advanced Siemens Fuel Rod Code," Enlarged HPG Meeting, Loen, May 19-24, 1996.

8. J. C. LaVake and M. Gaertner, "High Burnup PWR Ramp Test Program," Final Report DOE/ET/34030-10 CEND-420, December 1984 (work performed under contract DE-AC02-80 ET34030 for the United States Department of Energy).

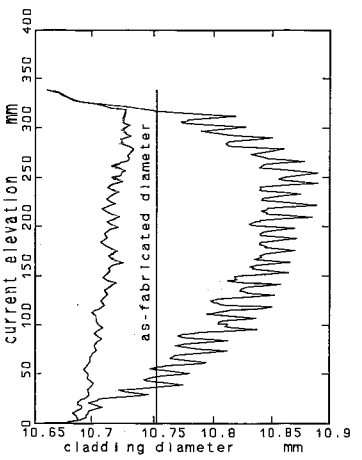


Figure 1a Super-Ramp PK2/3 Profilometry Prior To and After Ramp

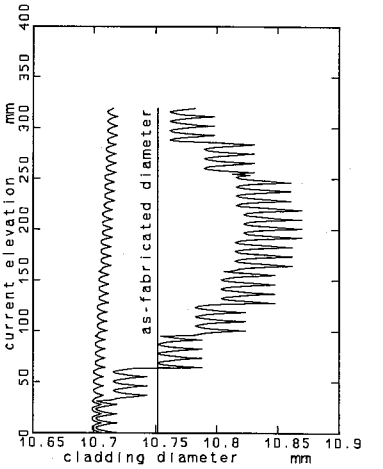


Figure 1b Super-Ramp PK2/3 Predicted Cladding Diameter Prior To and After Ramp

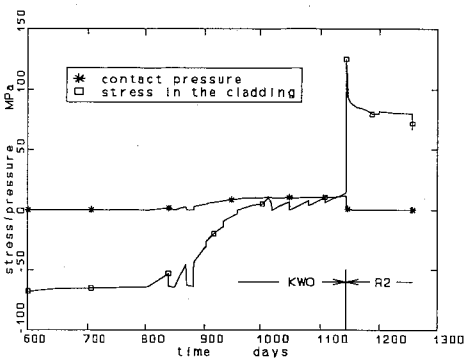


Figure 2a ROPE-II K1 Calculated Contact Pressure and Hoop Stress in the Cladding

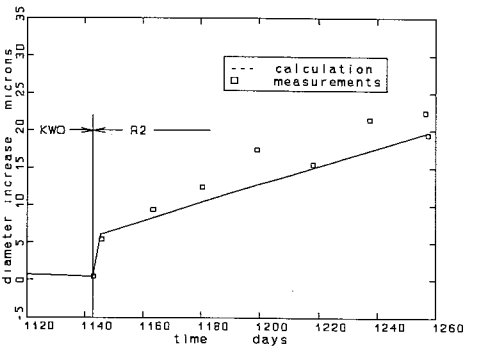


Figure 2b ROPE-II K1 Cladding Lift-Off in the R2 Reactor

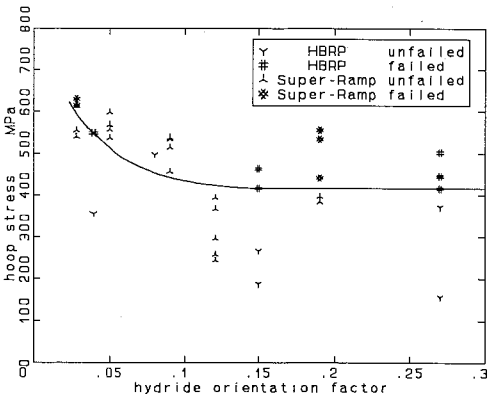


Figure 3 Failure Threshold in Terms of Hoop Stress Calculated with SIERRA

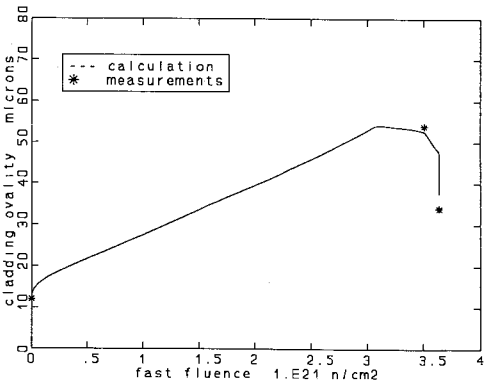


Figure 4 HBRP Rod 1/13 - Cladding Ovality Calculated with SIERRA

Transactions of the **14th International Conference on Structural Mechanics in Reactor Technology** (SMiRT 14), Lyon, France, August 17-22, 1997 **CW/3**

# Modelling the steady state and transient mechanical behaviour of fuel rods

**Garcia P., Moyne M.**
*CEA, France*

## ABSTRACT

Developing a fuel performance code which integrates increasingly mechanistic models is a step forward towards a comprehensive understanding of pellet cladding interaction (PCI). It is in this frame of mind that two models have been developed and integrated to the METEOR/TRANSURANUS fuel performance code, one pertaining to the mechanical behaviour of the fuel and cladding, the other to transient fission gas behaviour. The models are applied to calculate a base irradiation in a PWR and a subsequent power ramp experiment.

## INTRODUCTION

The ultimate aim of most fuel performance codes is to assess whether, under certain operating conditions, the fuel element cladding runs a risk of failing. This ambitious goal is made all the more difficult because of the myriad of complex phenomena that occur in a fuel rod. Although a multi dimensional analysis would no doubt yield information invaluable for interpreting, on the scale of a fuel pellet, observed changes in the fuel rod geometry (i.e. primary and secondary ridging), we will see that a mono-dimensional approach provides a useful frame work for circumscribing important mechanisms.

The purpose of this paper is to illustrate how two important models can be used to accurately reproduce original experimental results, thus validating our representation of the basic mechanisms.

Most fuel performance codes describe fuel pellets and cladding as axi-symmetric monolithic blocks. However, such an approach leads to the calculation of high tensile hoop and axial stresses in the fuel periphery, which are at odds with reported $UO_2$ fracture stresses[1].

A first approach led to the use of a correlation between the Young's modulus and the Poisson ratio of the fuel and the assumed number of radial cracks (i.e. parallel to the radial direction) in the fuel [2] (usually four). One of the main drawbacks to this approach is that the calculated pressure exerted by the expanding fuel on the zircaloy cladding in the case of a mechanical interaction is highly dependent on the value used in the numerical simulation for the elastic modulus of the fuel. The approach outlined in [2] leads to a reduction in the elastic modulus of the fuel which in turn can result in the underestimation of cladding strains. Furthermore, in Jankus and Weeks's analysis, the hoop and axial stresses remain tensile in the fuel periphery. Finally, it may be useful to establish a more realistic stress distribution in the

fuel if one's aim is to model phenomena such as creep or fission gas swelling which are notoriously stress dependent.

Oxide fuel pellets are known to be brittle especially at low temperature. Because of the temperature profile in a fuel rod, cracks are initiated in the outer rim area of the pellet and tend to propagate inwards as the linear power increases. This is generally thought to occur at around 60W/cm. As the cracks propagate, stresses in the fuel are relieved and the stress in the direction perpendicular to a crack drops to a value which is determined by the pressure in the fuel rod. A simple model has been developed based on these observations. It describes stress relaxation phenomena such as cracking and creep of fuel and cladding creep.

The first part of this paper deals with the mechanical model itself and the hypotheses that underlie it. The second part pertains to the mechanistic fission gas release model applied to describe transient gas behaviour. We then go on to apply both models to the calculation of the GONCOR analytical power ramp experiment performed in the SILOE test reactor.

## 1-MECHANICAL MODELLING

The basic assumptions chosen for the mechanical analysis are those usually applied to fuel performance codes that model the integral behaviour of a fuel rod ([3], [4]). The mechanical model represents the fuel element (fuel and cladding) as a series of regions for which an axisymmetric, isotropic and 'generalised' plane strain analysis is performed (Fig.1). Plane strain conditions are assumed to apply since the pellet radius is small in comparison to the total length of the fuel rod. Shear stresses in the fuel vanish as a consequence of the axi symmetric assumption and the only remaining stress and strain components are those in the r, $\theta$, and z directions (i.e. the principal axes of stress). They are noted $\sigma_r$, $\sigma_\theta$, $\sigma_z$, $\varepsilon_r$, $\varepsilon_\theta$, $\varepsilon_z$ in the remainder of this paper.

### *1-1 Basic equations*

From the above hypotheses, one can derive the basic equations that govern the mechanical behaviour of an axial slice. The stresses $\sigma_r$ and $\sigma_\theta$ satisfy the radial equilibrium equation :

$$r\frac{d\sigma_r}{dr}+\sigma_r-\sigma_\theta=0 \qquad (1)$$

In cylindrical coordinates, the strains in the r and $\theta$ directions are related to the radial displacement field u, by the following relations :

$$\varepsilon_r=\frac{du}{dr},\varepsilon_\theta=\frac{u}{r} \qquad (2)$$

An important assumption is that the total strain is obtained by summing all elementary contributions (elastic and non-elastic), i.e. :

$$\varepsilon_{r,z,\theta}=\varepsilon^{elas.}_{r,z,\theta}+\varepsilon^{n.elas.}_{r,z,\theta} \qquad (4)$$

The second term on the right hand side of equation (4) refers to the sum of all non elastic contributions.

Finally, Hooke's law is used to derive the relation between stress and strain at a given point in the structure :

$$\begin{pmatrix}\sigma_r\\ \sigma_\theta\\ \sigma_z\end{pmatrix}=\frac{E}{(1+\nu)(1-2\nu)}\begin{pmatrix}1-\nu & \nu & \nu\\ \nu & 1-\nu & \nu\\ \nu & \nu & 1-\nu\end{pmatrix}\cdot\begin{pmatrix}\varepsilon^{elas.}_r\\ \varepsilon^{elas.}_\theta\\ \varepsilon^{elas.}_z\end{pmatrix} \qquad (5)$$

How the axial balance is treated, which depends on whether the fuel cladding gap is open or not will be seen later on.

*1-2 Fuel cracking*

Fuel cracking is widely recognised as being an efficient means by which stresses in the fuel pellet are relieved [5]. Cracking is also known to be the main cause of fuel relocation (e.g. [6]). This apparent increase in the diameter of a cracked pellet is due to the fact that cracks intrinsically occupy a certain volume, which the model presented in this section should at least partially account for. It can also be ascribed to the fact that fuel fragments move with respect to one another ([9]). This topic will be briefly discussed in the third part of the paper.

Whatever the motivation behind modelling fuel cracking, one could argue that if a radial crack appears, the supposed symmetry of revolution breaks down. An idealised view of a fuel fragment delineated by two consecutive radial cracks is presented in figure 2. Let $\theta$ be the angle indicated in figure 2. The assumption which underlies the model is that the hoop stress does not significantly deviate from the value it reaches on either side of the fragment, that is to say the value imposed by the boundary condition : $\sigma_\theta(r,\theta) \approx -P$, where P is the pressure in the fuel rod. In other words, if a radial crack appears, $\sigma_\theta$ is still treated as a function of the radial position only, which enables the analysis to retain its axisymmetric nature.

Radial cracks and axial cracks (i.e. perpendicular to the axis of symmetry) which appear as a result of the tangential or axial components of stress exceeding the fuel fracture stress, are modelled. In a given slice, the fuel is divided into meshes sufficiently small to suppose that there is little variation of the elastic properties of the material. Each mesh can therefore take on four distinct crack related configurations : a)-the mesh is not cracked (or cracks are closed); b) radial crack is open, axial crack closed; c) axial crack is open, radial crack is closed; d) axial and radial cracks are open.

Conditions b), c) and d) lead to, $\sigma_\theta = -P$, $\sigma_z = -P$ and $\sigma_\theta = \sigma_z = -P$ respectively; $\sigma_\theta$ and $\sigma_z$ being the tangential and axial stresses in the pellet.

For a given mesh, the differential equation governing the displacement field u is established. If the mesh is not cracked, then combining equations (1), (2), (4) and (5) yields :

$$(1-\nu).\frac{d}{dr}.(\frac{1}{r}\frac{d(u.r)}{dr})=(1-\nu)\frac{d\varepsilon_r^{n.elas.}}{dr}+\nu\frac{d(\varepsilon_\theta^{n.elas.}+\varepsilon_z^{n.elas.})}{dr}+\frac{1-\nu}{r}(\varepsilon_r^{n.elas.}-\varepsilon_\theta^{n.elas.}) \quad (6)$$

In equation (4), all non elastic strain components are known and since the fuel mesh is not cracked, the crack component of strain is zero. However, if the fuel is cracked in a particular direction, the value of the stress component in the corresponding direction is worth -P. The unknown therefore switches from being a component of stress to a component of strain. To illustrate this, we consider the three remaining cases listed above. Combining equations (1), (2) and (4) with the appropriate crack related conditions ($\sigma_\theta = -P$, $\sigma_z = -P$ or $\sigma_\theta = \sigma_z = -P$) yields the three following differential equation:

$$\frac{d}{dr}(r\frac{du}{dr})=\frac{dr(\varepsilon_r^{n.elas.}+\nu\varepsilon_z^{n.elas.})}{dr}-\frac{1+\nu}{E}P-\nu\varepsilon_z^{n.elas.} \quad (7)$$

$$\frac{d^2u}{dr^2}+\frac{1}{r}\frac{du}{dr}-\frac{u}{r^2}=\frac{d(\nu\varepsilon_\theta^{n.elas.}+\varepsilon_r^{n.elas.})}{dr}+\frac{1-\nu}{r}(\varepsilon_r^{n.elas.}-\varepsilon_\theta^{n.elas.}) \quad (8)$$

$$\frac{d}{dr}(r\frac{du}{dr})=\frac{dr\varepsilon_r^{n.elas.}}{dr}+\frac{1-2\nu}{E}P \quad (9)$$

The interesting point is that if the fuel is cracked in a particular direction, the cracking strains do not appear explicitly in the corresponding equation. This means that they may be computed by subtracting from the total strain, the sum of all known strains, both elastic and non elastic. It will be seen to be of significant importance later on.

*1-3 Fuel and cladding creep*

Fuel and cladding creep are treated implicitly, as a result of which pseudo elastic constants E* and v* are defined ([3]):

$$E^* = \frac{E}{1 + E.\Delta t.\frac{\dot{\varepsilon}}{\sigma_e}}, v^* = \frac{1}{2}\frac{2v + \frac{\dot{\varepsilon}}{\sigma_e}E.\Delta t.}{1 + E.\Delta t.\frac{\dot{\varepsilon}}{\sigma_e}} \tag{10}$$

where is $\dot{\varepsilon}$ the creep rate, and $\sigma_\varepsilon$ the Von Mises stress and $\Delta t$ the time step. An iterative scheme is applied so as to converge over a time step on a value of $\dot{\varepsilon} / \sigma_\varepsilon$. At high temperature however, the Von Mises stress in the fuel will quickly tend to zero, even if the three principal stresses are highly compressive, i.e.: $\sigma_\theta = \sigma_z = \sigma_r$. This defines a fifth possible state for a fuel mesh. The corresponding characteristic displacement equation is:

$$\frac{d}{dr}.(\frac{1}{r}\frac{d(u.r)}{dr}) = \frac{d(\varepsilon_r^{n.elas.} + \varepsilon_\theta^{n.elas.} + \varepsilon_z^{n.elas.})}{dr} \tag{11}$$

It is again interesting to point out that solving this equation does not require the use of the value of the visco-plastic strains in the mesh since creep is a deformation that occurs at constant volume (i.e. $\varepsilon_r^{creep} + \varepsilon_\theta^{creep} + \varepsilon_z^{creep} = 0$).

*1-4 Axial balance*

In a given slice, the axial balance equations applied are straightforward. Open and closed gap situations are treated differently. If the fuel-cladding gap is open, the fuel stack and cladding are treated separately and the balance of axial forces on a slice is expressed by two distinct equations that apply over the fuel or the cladding. If on the other hand, the fuel-cladding gap is closed, the fuel and cladding are assumed to be bonded and a single equation applies. In this case, an extra equation is added in accordance with the hypothesis that no relative axial movement between the fuel and cladding is allowed.

*1-5 Numerical solution*

To illustrate matters, the numerical scheme is described for the fuel only and in the case of an open gap. If $N_f$ is the number of meshes used to model a fuel slice, the problem lies in solving $N_f$ second order differential equations. Analytical solutions can be obtained for equations (6) through (9) and (11). The problem therefore boils down to computing $2.N_f$ integration constants in addition to the axial strain in the slice (the plane strain hypothesis implies that the axial strain is independent of the radius at a given axial location).

Calculating these $2N_f+1$ unknowns is done by writing the continuity conditions for the displacement and radial stress fields at the interface between two consecutive meshes. The three remaining necessary equations are obtained by applying the appropriate balance equation (see section *1-4*) and the two boundary conditions.

This analysis is performed for a given crack and creep related configuration in a slice. An iterative system is added to decide what state each fuel mesh is in. All fuel meshes are initially modelled as being un-cracked. If the hoop or axial stress computed in a given mesh exceeds the fuel fracture stress (assumed constant and worth 150MPa), the state of the mesh is changed to its appropriate value. If on the other hand a negative cracking strain is computed in a mesh, following a stress and strain calculation, the crack closes at that radial position. In either of these cases the mechanical analysis of a slice is repeated until no mesh has changed states. Once convergence is attained, the creep analysis is performed.

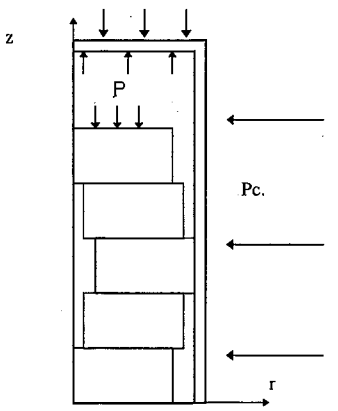


Fig.1 : Idealised view of a fuel element

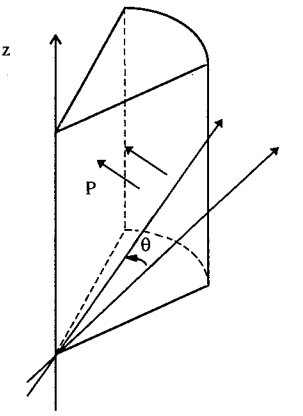


Fig.2:Idealised view of a fuel fragment

## 2-TRANSIENT FISSION GAS MODELLING

Describing how fission gases behave is essential to any detailed understanding of how fuel rods are loaded in the course of their irradiation history. Fission gas bubbles can swell either as a result of an influx of diffusing matrix gas atoms or because, if the fuel temperature rises, bubble motion and coalescence is possible.

It is however all the more significant to model fission gas release and swelling when simulating transient operating conditions because of the strong temperature dependence of diffusion mechanisms. A mechanistic model, based on [7], that describes the transient swelling and release of fission gases has been developed. Our aim is to outline the basic features and assumptions that underlie this model.

### *2-1 Basic assumptions.*

Three gas populations are modelled. They include intragranular and intergranular gas along with the interconnected grain-edge porosity. The intragranular population is divided into two categories. Fission gases are either present as dissolved atoms in the matrix or contained in initially small (nanometric) bubbles. The entire intergranular gas population is contained in bubbles, the concentration of which is a model parameter. At a given position in the fuel only a single bubble size is considered per population.

### *2-2 Gas release and transfer mechanisms-fuel swelling.*

Gas release from the fuel to the free volumes in the rod is described as a three stage process. Firstly, intragranular bubbles migrate to grain boundaries. The assumed mechanism is surface diffusion in a temperature gradient. The flow of grain boundary gas to the interconnected porosity then occurs if the estimated grain surface occupied by intergranular bubbles exceeds 30% of the total grain boundary surface area. The transfer kinetics from the grain boundary to the interconnected porosity is assumed to be proportional to the difference in pressure between the corresponding gas populations. Finally, the flow of gas through the

interconnected porosity to the free volumes which ultimately leads to its release is modelled as following a percolation law [8].

Only inter and intragranular swelling is considered. The interconnected porosity is thought to consist of relatively large pores which contain a low pressure gas. In other words, a change in the pressure in the cavity will not lead to a notable increase in its size. Hence its contribution to fuel swelling is neglected.

Intragranular bubbles coarsen as a result of both the influx of gas atoms from the matrix and of coalescence of moving bubbles. The fuel swelling computation is based on the calculation of the equilibrium bubble radius. This radius is obtained by solving the mechanical equilibrium equation which is expresses equilibrium between the inner bubble pressure, the surface tension of the solid and the calculated hydrostatic stress in the surrounding fuel. A Van Der Waals equation is used as equation of state for the gas. A similar treatment is applied to intergranular swelling, only bubbles are described as taking on a lenticular shape.

## 3-MODEL APPLICATION

### *3-1 Introduction*

The aim of this section is twofold. It serves to illustrate the sort of information the models presented in this paper can yield but also to ascertain whether the basic mechanisms accounted for are at all relevant. Fuel behaviour codes are usually validated against global post irradiation experimental results. In pile monitoring of useful experimental information is seldom possible. However the DECOR rig installed in the SILOE test reactor enables in-pile cladding diameter measurements. The installation is described elsewhere [9]. The GONCOR experiment ([10]) was carried out in the rig and involved re-fabricating a small section of fuel rod (previously irradiated in an EDF power reactor to a relatively high burn-up) and submitting it to a power ramp test. The experiment was designed to quantify the effect of high burn-up fission gas induced fuel swelling and fission gas release. The coupled mechanical and fission gas behaviour models have been integrated to the METEOR/TRANSURANUS code and applied to interpret the main experimental features of the GONCOR power ramp.

### *3-2 Results and discussion*

The original fuel rod was subjected to a standard power history with the maximum linear rating raging between 150W/cm and 250W/cm over four irradiation cycles. The calculated local burn-up reached is approximately 48GWd/t. The only steady state model which had to be adjusted for numerical simulation of the base irradiation was the fuel relocation model. Fuel relocation has been extensively studied and is regarded as being a consequence of fuel fragments occupying more space than the initially un-cracked pellet. Applying the cracking model presented in section 1 does not avoid the use of a fuel relocation model, but it was interesting to note that the relocation strain had to be decreased in order to predict gap closure kinetics in line with those predicted by the reference version of the code. One can ascribe this to the propensity of the mechanical behaviour model to partially simulate the increase in pellet diameter due to cracking.

Fig. 3 shows the power ramp history. After an initial rise to 250W/cm, the linear power was increased to around 400W/cm and held, all but for three power changes, for approximately six days. Also indicated in figure 3 is a comparison of the measured and calculated cladding diameter changes at the axial location where the neutron flux (hence

linear power) is maximum. Values indicated in figure 3 were measured at three adjacent axial positions: on a primary ridge, on a secondary ridge and in between both ridges.

Secondary ridging is indeed typical of the effect of power ramps on moderate or high burn-up fuel rods. Although there is a wide consensus regarding the cause of primary ridging (namely 'hour-glassing', e.g. [11]), the exact cause behind the onset of secondary ridging is still in the main unidentified. A possible explanation could be that fuel swelling and creep at high temperature lead to the filling of dishes at both ends of the pellet. This may substantially limit the cladding diameter increase at the interface between two pellets. As one moves away from the interpellet, the effect of dish filling recedes. The fact that the mid-pellet behaviour is less influenced by the presence of pellet dishes could explain the close agreement between our model calculation and the diameter changes measured at secondary ridge positions.

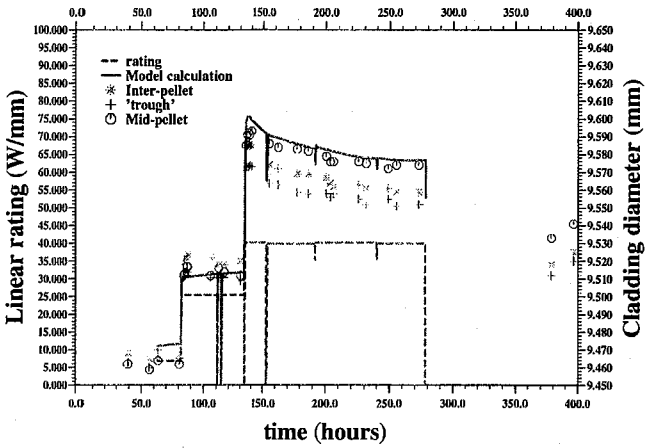


Fig. 3: Comparison of measured and calculated cladding diameter changes

We will now proceed to interpret the characteristic change in cladding diameter illustrated in figure 3. The initial sharp increase is due to fission gas swelling as a result of the activation of diffusion processes. The cladding diameter then reaches a maximum as the intergranular gas begins to flow from the grain boundaries to the interconnected porosity network. The fuel then gradually deflates as the interconnected porosity gas percolates out of the fuel.

Quantifying both the overall effect of fuel swelling and the corresponding kinetics is made possible by comparison of experimental and model calculation results. A simple thermo-elastic calculation shows that the effect of swelling (at 400W/cm for a 48GWd/t fuel rod) is a diameter increase that ranges between 30μm and 50μm. Our calculations also show that after 15mn at 400W/cm, the cladding diameter increase, for a power increase from 250W/cm to 400W/cm, has reached 85% of its maximum value. This is indicative of the importance of fission gas behaviour on cladding loading in transient conditions.

The calculated overall fission gas release is in good agreement with PIE results. Measured values are estimated at 25% ([10]) and the calculated value is 26.8%. The metallographic examinations also corroborate model calculations. These reveal a circular ring of intragranular bubbles located between 71% and 65% of the outer pellet radius [10]. The fission gas model predicts a drop in intragranular gas concentration, at the end of the experiment, that spreads over an area located between 73% and 70% of the pellet radius. Calculations predict that the temperature of the outer part of this zone varies between 1020°C and 1100°C, which is high enough for bubble nucleation to occur but too low to result in any appreciable bubble movement.

## 4-CONCLUSION

Two models one pertaining to the mechanical behaviour of fuel rods and the other to transient fission gas swelling and release have been assessed against results from an analytical experiment performed on a highly irradiated fuel rod. Calculations are in fairly good agreement with overall experimental results (cladding diameter changes and overall fission gas release) which purports to show that the essential mechanisms are properly accounted for. In particular, the characteristic change in cladding diameter during a power ramp is interpreted as an initial swelling and subsequent deflating of the fuel. However, the models presented in this paper need to be assessed over a wide range of burnups, maximum power ratings and hold times. There is no doubt that taking into account primary and secondary ridging along with the axial flow of fuel in the central part of the pellet is of the utmost importance if one is to succeed in comprehensively describing PCI.

## References


1. Guérin, Y. 1985. Le comportement mécanique du combustible sous irradiation.
Annales de. Chimie 10: 405-414.

2. Jankus V.Z. and Weeks R.W. 1972. Life II - a computer analysis of fast-reactor fuel-element behaviour as a function of reactor operating history.
Nuclear engineering and design 18: 83-96.

3. Lassmann K., Blank H. 1988. Modelling of fuel rods and recent advances of the Transuranus code.
Nuclear engineering and design 106: 291-313.

4. Struzik C., Mélis J-C., Fédérici E. 1994. Fuel modelling at extended burnup : comparison between calculation and examination on fuel rods irradiated up to 60000MWd/Ut.
Proc. ANS topical meeting: 188-195. West Palm Beach

5. Rashid Y.R. 1974. Mathematical modeling and analysis of fuel rods.
Nuclear engineering and design 29: 22-32.

6. Struzik C., Moyne M., Piron J-P. 1997. High burnup modelling of UO2 and MOX fuel with Meteor/Transuranus.
Proc. ANS topical meeting. Portland. To be published.

7. Cranga M. 1983. The treatment of gas in the COSAG model, part of the safety code Physura.
Proc. Fission gas behaviour in safety experiments-Cadarache.

8. Hoffman J.R., Meeks C.C. 1977. Internal pressurization of solid mixed-oxide fuel due to transient fission gas release.
Nuclear science and engineering 64: 713-723.

9. Caillot L., Delette G., Julien B., Couty J-C. 1997. Contribution de la fragmentation à l'IPG dans un crayon de REP : programme expérimental RECOR.
Proc. This conference.

10. Caillot L., Delette G. Work to be published.

11. Iwano Y. 1988. Simple model for analysis of circumferential ridging deformation of fuel rods.
Journal of nuclear science and technology 25: 368-376.

Transactions of the **14th International Conference on Structural Mechanics in Reactor Technology** (SMiRT 14), Lyon, France, August 17-22, 1997 **CW/4**

# Nonlinear finite element studies of the pellet-cladding mechanical interaction in a PWR fuel

**Brochard J., Bentejac F., Hourdequin N.**
*CEA, France*

ABSTRACT : After a presentation of the general features of the code TOUTATIS, which is a specific module of the FEM code CASTEM2000 developed in the framework of the CEA project METEOR to describe the local thermomechanical behaviour of PWR fuel rods, results of a parametric study conducted in order to analyse the influence of some modelling assumptions and of the pellet geometry on PCMI intensity are shown. Accurate modelling of the axial pellet-clad constraints and of the pellet fragmentation is proved to be important.

## 1. INTRODUCTION

In order to simulate accurately the local mechanical behaviour of PWR fuel rods during steady-state or power transient, a specific module of the general purpose finite element computer code CASTEM2000 is in progress. This code, TOUTATIS, based upon 2D or 3D models, is developed in the framework of the C.E.A. research and development project METEOR, as well as the 1D1/2 thermomechanical code METEOR/TU which is used to describe the global behaviour of a fuel rod [1]. Up to now, the developments of the code TOUTATIS have been focussed on the prediction of cladding tube failures by pellet cladding interaction (PCI) after an up power excursion (power ramp) [2], especially for fuel rods irradiated for 2 cycles in a power reactor, because for such fuel rods the configuration is favourable to PCI failures : the pellet-cladding gap is closed while the considered power transients occur. Many physical models are available in the global code METEOR/TU and an interface can be used to transfer data from the global code to improve the local modelling.

This paper presents the results of a parametric study conducted in order to quantify the influence of modelling assumptions such as pellet fragmentation or pellet-cladding friction on the amplitude of the predicted cladding ridges after the transient. The calculations were performed with the material properties and the cold pellet-cladding gap of a 2 cycle fuel rod. The influence of the pellet geometry on the pellet cladding mechanical interaction (PCMI) has been analysed also.

## 2. DESCRIPTION OF MODELS

In a first step, an axisymmetric model has been developed. Usually the mesh is limited to one half of a pellet with the adjacent cladding part (figure 1).

The appropriate boundary conditions on the pellet and the cladding are indicated on fig. 1 :

- Contact condition at pellet - pellet interface, dish closure being permitted : $Uz(r) + h(r) \geq 0$
- Condition to treat the pellet midsection plane as a plane of symmetry : $Uz = const.$

- Corresponding symmetry conditions for the cladding : Uz = 0 and Uz = const. respectively at the bottom and at the top of the model.
- Radial contact condition at pellet-clad interface : $Ur_{pellet} \leq gap + Ur_{clad}$

Two extreme axial constraints are proposed for the pellet - clad interface :
- Locking condition after the initial pellet-clad contact : $\Delta Uz_{pellet} = \Delta Uz_{clad}$ at midsection and interface planes.
- No pellet-clad axial constraint.

For steady-state conditions, as well as for ramp transient, the code takes into account :
- The mechanical loads : fuel pellet compression spring force, internal gas pressure (up to now without fission gas release), external coolant pressure.
- The fuel temperatures calculated using the gap conductance updated with the thermally expanded geometry and with or without flux depression.

The stresses and strains are calculated using non linear resolutions taking into account creep and plasticity for $UO_2$ and Zy4. Fuel swelling is also considered for its contribution to reduce the gap size with burn up [3].

The axisymmetric model can display the typical "diabolo" shape of the pellet due to the quasi-parabolic fuel temperature distribution, nevertheless this model under-estimates the amplitude of the permanent clad ridges after a power ramp.

To improve the prediction of the cladding deformation, it is necessary to take into account the pellet fragmentation. So, in a second step, a tridimensionnal model, with an idealised fuel fracture pattern, has been developed. Usually the pellet is supposed precracked into four (or eight) equal fragments by four (or eight) radial cracks extending to the fuel center line. The mesh is limited to one fragment using the previously described boundary conditions with additional contact conditions at fragment-fragment planes and corresponding symmetry conditions for the cladding (figure 2) . At the pellet-clad interface, the sliding condition is the unique available condition in the current version. This model supposes preexistent pellet fractures before irradiation : this modelling assumption is justified because the oxide fracture occurs at low heat generation level. Furthermore, a previous analysis showed up that the idealised model of the pellet completely cracked to the centerline gives similar results than a more complex model for which the pellet crack pattern is determined by the $UO_2$ fracture stress [4].

## 3. METHODOLOGY FOR A POWER RAMP CALCULATION

A brief description of the methodology to calculate a power ramp for a 2 cycle fuel rod is given below. At the present state, it is applied with the 2D model.

In order to start the ramp calculation with a correct initial state, the two irradiation cycles are modelled. The calculation is divided in several periods (usually 10 to 15 periods per cycle) during which material properties and loads are supposed constant. At the beginning of a new period thermal resolutions are performed to determine the new temperature distributions taking into account the updated gap conductance and material properties. The internal gas pressure is also updated with the new gap temperature and the reduced free volumes evaluated on the actualised geometry. This estimation is done supposing the behaviour of all fuel rod pellets identical : this assumption is correct for an irradiation in a power reactor because the axial shape factor is almost flat. Therefore the internal pressure evolution can be transferred from a global calculation using the code METEOR/TU. Each period is subdivided in several time steps with successive nonlinear mechanical resolutions to simulate the following mechanisms :
- gap size reduction due to the combined effects of the fuel swelling and clad diameter reduction by creep under the differential external pressure,

- clad ridges at the pellet interface by PCMI when the gap is closed.

The final stress and strain fields at the end of the base irradiation are introduced as initial state for the power ramp calculation. Because of the severe loading during the ramp, plastic strains can't be neglected. To take into account both plastic and creep strains, the linear power increase is approximated by a succession of power steps with plasticity during instantaneous power increments and creep during hold periods. Usually a 200W/cm power increase is divided in 10 power increments with constant hold periods. Hold periods are adjusted to the power rate. A typical input power history is shown in figures 3 and 4. The calculated clad inner surface hoop stress at the interface plane is presented on figures 5 and 6. At the end of the 1st base irradiation cycle, the hoop stress variation indicates that PCMI occurs. During the ramp, for a linear power rate equal to 100W/cm/min, a stress relaxation is observed at high power levels.

This analysis is going on to define a ramp calculation methodology using the 3D model. It has been mentioned previously that a data interface from the 1D1/2 code METEOR/TU to the 2D-3D code TOUTATIS is available. In fact, at the present state, some models, like the fission gas swelling or the fission gas release, are not taken into account in the ramp calculations. Some of these models require a global modelling and a reflection has been engaged to define the set of data it would be useful to transfer from the 1D1/2 code METEOR/TU to improve the numerical predictions using the local FE modelling.

## 4. SENSITIVITY STUDIES

In the following, results of sensibility studies to modelling assumptions or pellet geometry are presented. Calculations were performed for a power rate of 35 W/cm/min and peak final power 450W/cm kept for 3 min. The material properties and gap size correspond almost to a 2 cycle fuel (table 1). Stresses and strains due to the base irradiation are neglected and calculations simulate only the transient. These conditions might be representative of an irradiation on a fuel rod with a small initial diameter and for which PCMI don't occur during the base irradiation.

Preliminary, based on an average $UO_2$ fracture stress of about 115MPa, the power level corresponding to radial pellet fragmentation has been evaluated with the isovalues $\sigma_{\theta\theta}$ obtained by a 2D calculation for a standard pellet (H/D = 1) : about 100 W/cm (figure 7).

### *4. 1 Sensitivities to modelling assumptions*

Influence of the axial constraint on the PCMI prediction has been analysed simulating, with the 2D module, the two extreme cases described previously (§2) : "locked" condition or sliding condition. Results are presented on figures 8, 9 and 10.

Effect of the biaxiality of the loading is important : there is a multiplicative factor ranging from 2 to 7 on the amplitude of the permanent diameter expansion when the clad axial tension is taken into account.

The very low strain hardening of the clad stress-strain curve explains the equivalent stress saturation on figure 8. The ridge amplitude is reduced with the locked condition. However, approximation of the oxide Zy4 friction effect by equal axial displacement increments just at the ends of the pellet instead of all along the interface can accentuate this biaxiality effect.

Because it simulates the two following mechanisms :

- hoop stresses are cut at the fragment interface,
- fragments move away each other in the circumferential direction because of the fragment interface bulging,

the 3D model, with pellet fragmentation, gives a better representation, than the 2D one, of the radial expansion of the pellet subjected to the thermal gradient.

The comparison of predicted radial clad displacements using the 2D and 3D models is presented in figure 11. When the pellet fragmentation is taken into account, a significant clad deformation increase is showed up which corresponds to a clad permanent deformation increase after unloading.

*4.2 Sensitivities to the pellet geometry*

Influence of H/D ratio on PCMI intensity has been studied performing 3D ramp calculations with different pellet heights corresponding to H/D ratio ranged from 0,5 to 3. Figure 12 presents the comparison of the radial clad displacements at the power peak. A remarkable PCMI reduction is observed with a small pellet (H/D = 0,5). The maximal PCMI intensity is yielded for H/D ratio equal to 1 therefore for higher H/D ratios the reduction at pellet interface plane is balanced by an increase at the midsection plane.

Among the different kinds of pellet, we compared :

- a perfectly cylindrical pellet,
- a pellet with dishes,
- a pellet with chamfers,
- a hollow pellet.

The 3D ramp calculations were performed with a H/D ratio equal to 1. Results are presented on figure 13. For an identical thermal flux at the pellet-clad interface, temperatures in the pellet are lower for the hollow pellet. The pellet thermal expansion and consequently the PCMI are reduced for the hollow pellets. Differences between the other cases are minor.

## 5. CONCLUSION

To complete the 1D1/2 code METEOR/TU which is devoted to the fuel rod global behaviour, the development of the 2D-3D code TOUTATIS, based upon the FEM code CASTEM and devoted to the refined mechanical analyses, is in progress. Efforts are undergone to improve the PCI modelling for fuel rods subjected to a power ramp, especially for 2 cycle fuel.

Among the parameters which can influence the PCMI intensity, the pellet-clad axial constraints and the pellet fragmentation have been identified.

Using the 3D module, parametric calculations have been performed to analyse the influence of the pellet geometry. Important PCMI reductions are identified for short pellets and hollow pellets. These two cases being excluded, the differences are not so significant, therefore a larger effect has been noticed with the H/D ratio.

## REFERENCES


1. Struzik, C., J.C. Melis & E. Federici 1994. Fuel modelling at extended burn-up : comparison between METEOR/TRANSURANUS calculations and examinations on fuel rods irradiated up to 60 GWd/tU.
   *Proc. 1994 International Topical Meeting on light water Reactor Fuel Performance* : 188-195. West Palm Beach, Florida.
2. Caillot, L., B. Linet & C. Lemaignan 1993. Pellet clad interaction in PWR fuel : analytical irradiation experiment and finite element modelling.
   *Proc. 12$^{th}$ International Conference on Structural Mechanics In Reactor Technology* : C04/2. Stuttgart, Germany.

3. Hourdequin, N. 1995. Contribution à la modélisation du comportement mécanique des combustibles REP sous irradiation, avec en particulier le traitement de l'interaction pastille-gaine dans un crayon combustible. *CEA-R-5709.*
4. Hering, W., I.B. Fiero & S. Darling 1979. Sensitivity of power ramp induced cladding stress and strain concentrations to modelling assumptions. *Proc. 5th International Conference on Structural Mechanics In Reactor Technology* : D2/4. Berlin, Germany.
5. Harding, J.H. & D.G. Martin 1989. A recommendation for the thermal conductivity of $UO_2$. *Journal of Nuclear Materials 166* : 223-226.
6. Petitgrand, S. 1980. Predictions of the thermomechanical code «RESTA» compared with fuel element examination after irradiation in the BR3 reactor. *Specialists' meeting on fuel element performance computer modelling, IAEA International Working Group on Fuel Performance and technology for Water Reactor* : 210-216. Blackpool, U. K.
7. Lassmann, K. & F. Hohleferd 1987. The revised URGAP model to describe the gap conductance between fuel and cladding. *Nuclear Engineering and Design 103* : 215-221.
8. Martin, D.G. 1990. *Catalogue Européen des Propriétés de l'Oxyde Mixte (U, Pu)$O_2$.*
9. Canon, R.F., J.T.A. Roberts & R.J. Beals 1971. Deformation of $UO_2$ at high temperatures. *Journal of the American Ceramic Society 54* : 105-112.
10. Otter, C. 1976. *CEA.*

| | | |
|---|---|---|
| GEOMETRY | $H/D_{pellet}$ ratio | 1 |
| | $D_{dishes}/D_{pellet}$ ratio | 0,76 |
| | Diametral pellet-clad gap | $20.10^{-6}$ m |
| THERMAL MODELS | $UO_2$ conductivity | HARDING and MARTIN correlation [5] |
| | Zy4 conductivity | RESTA code model [6] |
| | Gap conductance | URGAP model [7] |
| MECHANICAL MODELS | $UO_2$ thermal expansion coefficient | MARTIN correlation [8] |
| | Zy4 thermal expansion coefficient | RESTA code model [6] |
| | $UO_2$ plasticity law | Linear cinematic strain hardening [9]<br>yield stress : $\sigma_{V.M.}(Pa) = 136.10^6 + 4{,}5.10^7\varepsilon_{eq.}$ |
| | $UO_2$ creep law | Inelastic deformation rate [10]:<br>$\dot{\varepsilon}_{eq.} = e^{\alpha P}A\left(\phi, D, \sigma_{eq.}\right)e^{-a/T} + e^{\beta P}\sigma_{eq}^{4,5}B(\phi)e^{-b/T} + \sigma_{eq.}k\phi e^{-c/T}$ |
| | Zy4 plasticity law | Linear cinematic strain hardening :<br>yield stress : $\sigma_{V.M.}(Pa) = 435.10^6 + 837.10^6\varepsilon_{eq.}$ |
| | Zy4 creep law | 2 cycle irradiated Zy4, short time, high stress :<br>inelastic deformation: $\varepsilon_\theta = A_2(\sigma,T)\left(1-e^{-R_2(\sigma,T)t}\right) + B_2(\sigma,T)t$ |

Table 1 : Geometrical characteristics and models used for sensitivity studies with TOUTATIS 2D-3D

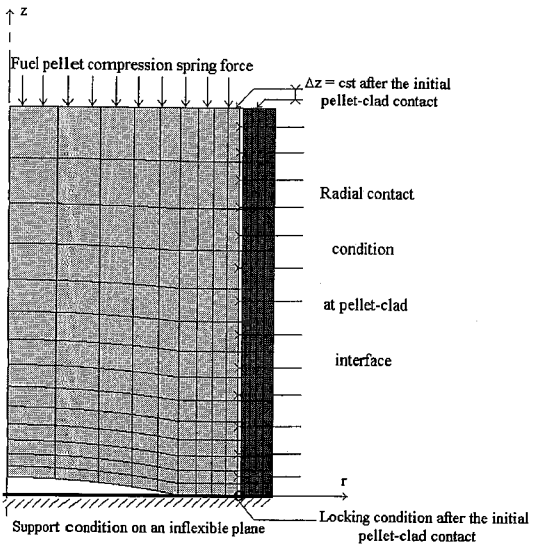


FIGURE 1 - 2D MODEL

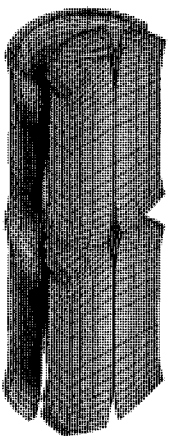

FIGURE 2 - 3D DEFORMED MODEL

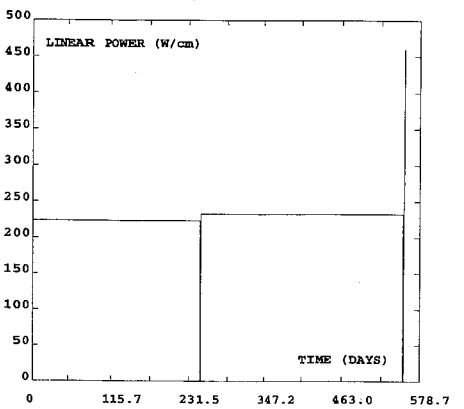


FIGURE 3 - TYPICAL POWER HISTORY : 2 CYCLE IRRADIATION PLUS POWER RAMP

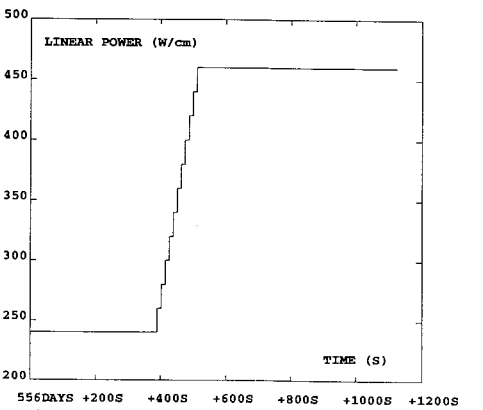


FIGURE 4 - MODELLED POWER HISTORY : FOR A POWER RAMP

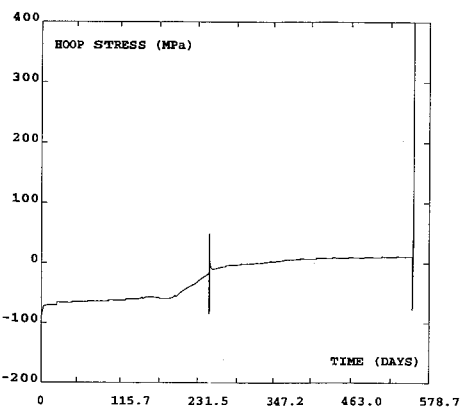


FIGURE 5 - CALCULATED INNER CLAD HOOP STRESS : 2 CYCLE IRRADIATION PLUS POWER RAMP

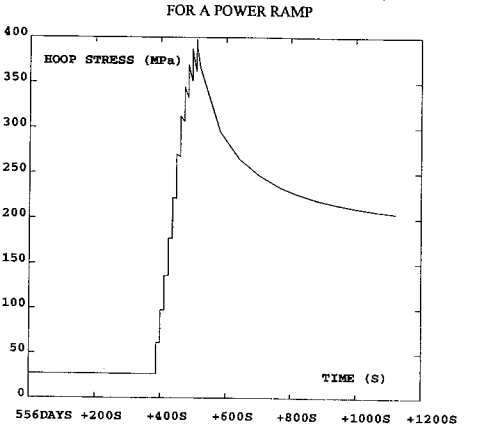


FIGURE 6 - CALCULATED INNER CLAD HOOP STRESS : POWER RAMP

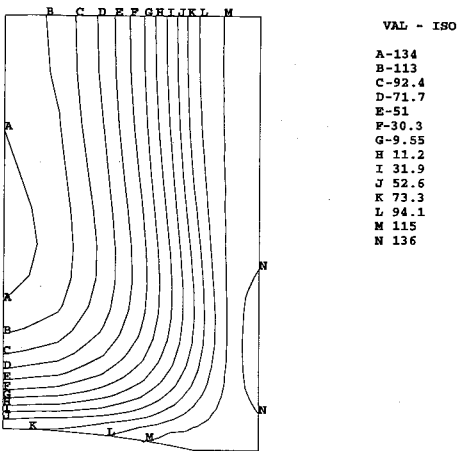


FIGURE 7 - HOOP STRESS ISOVALUES (MPa)
FOR A LINEAR POWER LEVEL OF 100 W/cm

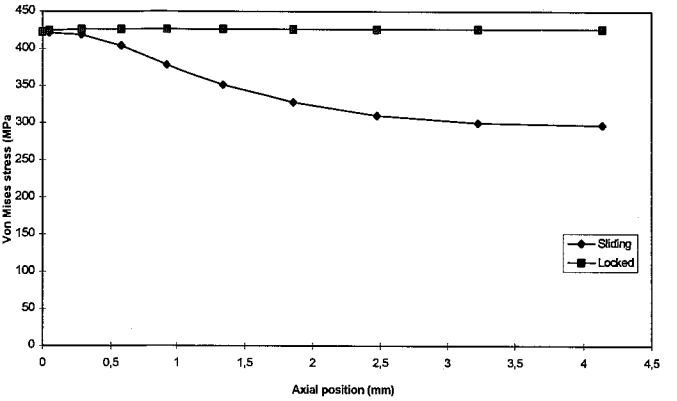


FIGURE 8 - CLAD VON MISES STRESS AT POWER PEAK CALCULATED WITH AXISYMMETRIC MODEL
FOR LOCKED AND SLIDING CONDITIONS

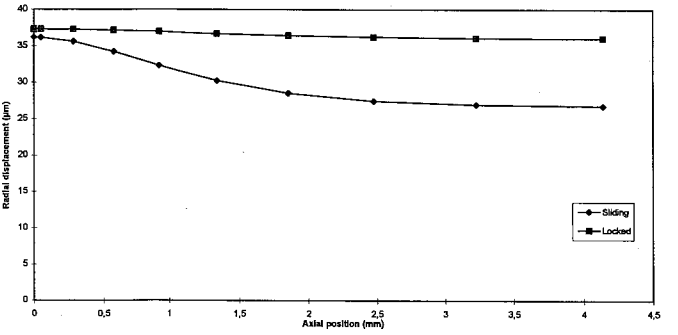


FIGURE 9 - CLAD RADIAL DISPLACEMENT AT POWER PEAK CALCULATED WITH AXISYMMETRIC MODEL
FOR LOCKED AND SLIDING CONDITIONS

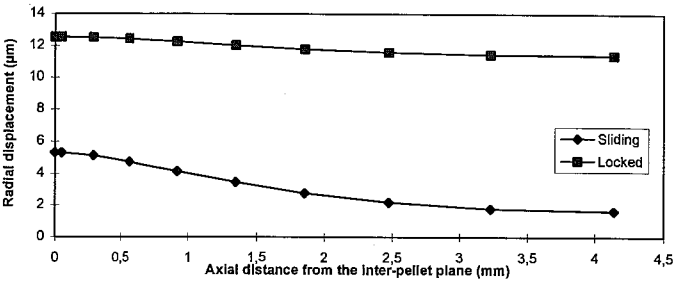


FIGURE 10 - CLAD RADIAL DISPLACEMENT AFTER UNLOADING CALCULATED WITH AXISYMMETRIC MODEL FOR LOCKED AND SLIDING CONDITIONS

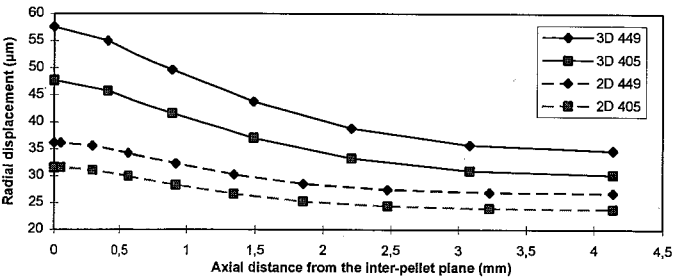


FIGURE 11 - CLAD RADIAL DISPLACEMENT AT POWER PEAK CALCULATED WITH AXISYMMETRIC AND 3D MODELS FOR SLIDING CONDITIONS

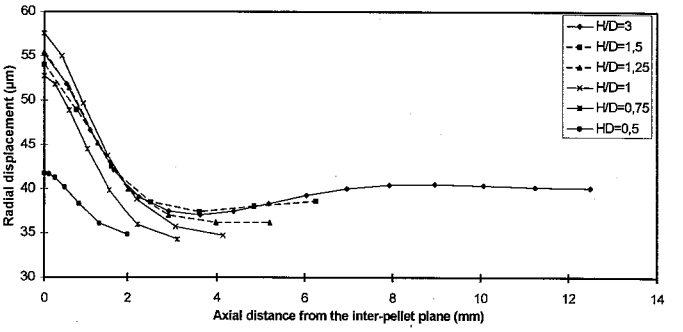


FIGURE 12 - CLAD RADIAL DISPLACEMENT AT POWER PEAK CALCULATED WITH 3D MODEL FOR VARIOUS H/D RATIOS

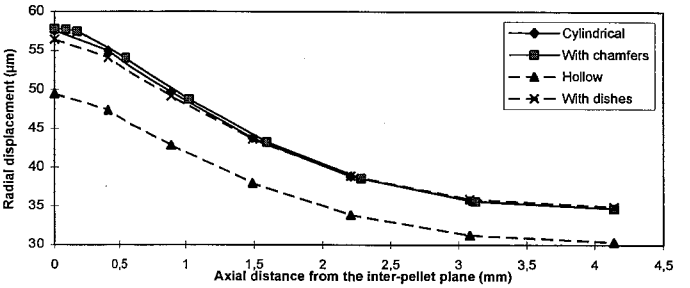


FIGURE 13 - CLAD RADIAL DISPLACEMENT AT POWER PEAK CALCULATED WITH 3D MODEL FOR VARIOUS PELLET GEOMETRIES

Transactions of the **14th International Conference on Structural Mechanics in Reactor Technology** (SMiRT 14), Lyon, France, August 17-22, 1997 **CW/5**

# Modelling of the fuel mechanical behavior : from creep laws to internal variable models

**Leclercq S.**
*EDF, France*

ABSTRACT : Creep laws such as Bohaboy's one are nowadays commonly used to simulate the fuel pellet response to the sollicitations it faces during its life. These laws are sufficient for describing the base operating conditions (where only creep appears), but they have to be improved for power ramp conditions (where hardening and relaxation appear). The aim of the present paper is to develop a framework in which it could be possible to build models more representative of the fuel pellet in pile sollicitations.

## 1. INTRODUCTION

The integrity of nuclear fuel rods is one of the major concern for companies like EDF and must be demonstrated, essentially for class I (normal) and II (incidental) operating conditions. As a matter of fact, one potential failure mode of the cladding is the so called Pellet/Cladding Mechanical Interaction which is normally induced by a power ramp. Moreover, the will to extend the fuel's life above four years leads to a need for a better understanding and simulation of the irradiation effects on the fuel mechanical behavior. Thus it clearly appears that the mechanical properties evolution of the cladding, as well as those of the fuel, have to be well known in order to cope with the needs in nuclear fuel rod mechanical modelling, in particular to gain some freedom degrees in nuclear power plants operating conditions. The choice of laws describing such properties remains the major problem.

The problem of determining constitutive equations of any material consists in two steps. First, one has to clearly identify the type of tests that are representative of the real mechanical behavior of the structure. Then the constitutive equations must be written and calibrated on the basis of these experimental results.

The constitutive equations at present existing in the different codes are roughly of the same type. They consist in the writing of a strain rate non linearly depending on the applied stress. Equations such as $\dot{\varepsilon} = f(\sigma^n)$ are often used. The exponent of the stress depends on the type of physical mechanism which is involved in the system. Those kinds of constitutive equations are commonly called creep laws, and are able to describe the way the strain increases at constant stress. These contitutive equations provide good predictions of the mechanical behavior of the nuclear fuel rod in normal operating conditions, but are not sufficient to describe the complete mechanical behavior, in particular from the viewpoint of hardening (or softening) properties and relaxation tests. Indeed, even if the creep properties are activated during the normal operating conditions of the nuclear power plant, it is clear that one cannot

assume that the stress remains constant, in particular for ramp conditions. In this case, mechanisms as hardening (or softening) and relaxation are also involved. Usually, the strain-hardening assumption is postulated to solve this problem. Nevertheless, the particular effects associated with relaxation may not be correctly simulated by such correction. Thus one needs constitutive equations that are able to predict such phenomena.

On the other hand, several physical mechanisms arise during the fuel pellet life, that are not *strictly* related to the mechanics, but that have a strong influence on the mechanical behavior of the material during its life. For instance, densification and gas swelling play a major role on the local mass density by changing the porosity inside the material, and hence have an influence on the non-linear rate of viscous deformation. In the actual codes simulating the fuel behavior, these mechanisms are taken into account apart from the mechanical behavior. That is, the deformations induced by densification and gas swelling are parts of the total deformation, but are calculated with no account for the interactions between porosity and viscosity. Thus, the viscoplastic deformation does not depend on the evolution of the porosity, which depends highly on the temperature and the stress field.

Hence, in this case, it seems more accurate to use models that are devoted to this particular behavior, in order to improve the simulation capability of the codes.

In the frame of the Thermodynamics of Irreversible Processes, it is now possible (and of classical use in several fields of mechanical research) to build up models based on the existence of internal variables, able to account for different aspects of the materials mechanical behavior [1]. These methods have already been successfully applied by EDF to simulate the fuel rod Zircaloy cladding behavior [2]. It is proposed here to develop a frame in which such models could be used to describe the elastoviscoplastic behavior of the fuel pellet. In a first part of this paper, the general frame of the model is presented. It is shown how it complies with the second law of thermodynamics. The dependance of the non-linear deformation rate on the effects of swelling and densification is explicitely exhibited. In a second part, it is shown how easy it may be to take into account the irradiation (burnup) on the mechanical behavior thanks to such approach. And the last part of this paper highligths how the parameters of such constitutive equation may be identified. Indeed, this requires also the development of new experimental techniques considering that the integrity loss of the pellet as soon as irradiation proceeds, dismissing the use of standard compressive tests. To this aim, a microindentation machine is developped by TUI (Karlsruhe, Germany) and EDF [3].

## 2. DESCRIPTION OF THE MODEL

The model has been designed to represent the non-linear mechanical behavior of the fuel pellet, influenced by the effects of swelling and densification that arise at different moments during the life of the fuel rod. The effects of irradiation (i.e. burnup effects) may also be introduced into the present model.

One will use the classical framework of the thermodynamics of irreversible processes to derive the equations described below. In particular, the dissipation aspects will be taken into account on the basis of the Clausius-Duhem inequality, with no direct reference to the classical dissipation potential used in the case of standard materials.

### 2.1 *The general layout*

Let us consider a representative volume V of the material in question. As the fuel material (a ceramic obtained by sintering of the Uranium oxide powder) is known to be porous, we define the porosity z as the ratio between the volume of pores $V_f$ and the total volume V. It may change during the fuel's life due to densification (irradiation activated resintering) and gas swelling. Thus, (1-z) constitutes the volume fraction of "sound" material.

It is here assumed that the porosity can have any shape and distribution.

As a conclusion of the layout, one considers that the assumption of small strains is valid here, i.e., the total strain is assumed to be of the form

$$\underline{\varepsilon} = \underline{\varepsilon}^e + \underline{\varepsilon}^{vp}, \tag{1}$$

where $\underline{\varepsilon}^{vp}$ is the viscoplastic (non-linear) part of the deformation. Hence, $\underline{\varepsilon}^e$ is the elastic part of this deformation.

### 2.2 *Thermodynamic principles and constitutive equations*

#### 2.2.1 *Specific free energy of the system*

The Helmholtz specific free energy of the system which can be considered as a two-phase one is written as follows :

$$\Phi(\underline{\varepsilon}^e, z, T) = (1-z)\Phi_1(\underline{\varepsilon}^e, \varepsilon^{vp}, T) + z\Phi_2(\underline{\varepsilon}^e) + \Phi_{it}(z, T), \tag{2}$$

where $\Phi_1$ is the specific free energy of the homogeneous material :

$$\Phi_1 = \frac{1}{2}\underline{\varepsilon}^e \underline{\underline{L}} \underline{\varepsilon}^e + \Phi^*(\varepsilon^{vp}, T). \tag{3}$$

In this equation, T is the absolute temperature, and $\Phi^*$ the free energy correlated with dissipation aspects. $\underline{\underline{L}}$ is the fourth-order elasticity tensor, while $\underline{\varepsilon}^e$ is the second order elastic deformation tensor.

The term $\Phi_2$ represents the elastic energy stored inside the porosity due to the presence of gas. One assumes for simplicity that it is equal to the elastic energy ($\frac{1}{2}\underline{\varepsilon}^e \underline{\underline{L}} \underline{\varepsilon}^e$) stored in $\Phi_1$.

In equation (2), the term $\Phi_{it}$ is called *interaction free energy*. It represents the effects of the porosity upon the total energy of the system. In particular, it takes into account the discontinuities that arise in the strain field, and the relaxations occuring in the stress field when a porosity germinates and grows inside the material.

It is chosen, and this is only an assumption, that $\Phi_{it}$ may be of the simple form :

$$\Phi_{it} = z(1-z)F, \tag{6}$$

where $F$ could be a function (experimentally determined) of the burnup $BU$.

Note that such a non-convex form for the interaction energy has already been used for representing the exotic behavior of shape memory alloys undergoing solid-solid phase transformations [4]. One has to point out that this interaction energy reaches a maximum when z = 1/2.

Note also that the free energy of the system is the one of the "sound" material if there is no porosity, and is equal to zero if the volume fraction of porosity is 1 (in this case, there is no more material).

### 2.2.2 *A constitutive assumption*

It is now time to give a sense to the viscoplastic strain $\underline{\varepsilon^{vp}}$. In a first approximation, and following the experimental results available in the literature for non-irradiated material [5], the equivalent (in the sense of von Mises) strain rate can be assumed as follows :

$$\dot{\gamma} = \left(\frac{\bar{\sigma}}{K\gamma^{1/M}}\right)^N, \tag{7}$$

where $\dot{\gamma}$ is the rate of equivalent viscoplastic strain, $\bar{\sigma}$ the equivalent stress, and K, M, N are constants. This equation is commonly referred to as the Lemaître law [6].

Thus, the deviatoric part of the viscoplastic strain rate reads :

$$dev(\underline{\dot{\varepsilon}^{vp}}) = \frac{3}{2}\dot{\gamma}\frac{dev\underline{\underline{\sigma}}}{\bar{\sigma}}. \tag{8}$$

The equation (8) means that the strain rate complies with the normality rule, with possibility of an isotropic hardening, but without any kinematic hardening. This is a restriction which is assumed for this paper, but which can be relaxed in the future.

Let us now deal with the hydrostatic part of the viscoplastic strain. Indeed, in the present case, the volume fraction of porosity may change, but mass conservation is a fundamental principle. Thus, the mass density $\rho$ must change with respect to z. If $\rho_0$ is the mass density corresponding to $z_0$ porosity, one can easily derive the following :

$$\frac{1-z}{1-z_0} = \frac{\rho}{\rho_0}. \tag{9}$$

Moreover, neglecting the elastic part of the hydrostatic deformation rate, the equation of mass conservation reads : $\dot{\rho} + 3\rho\dot{\varepsilon}_m^{vp} = 0$, where $\varepsilon_m^{vp} = \frac{1}{3}tr(\underline{\varepsilon^{vp}})$.

This allows one to derive the constitutive equation for the viscoplastic strain rate :

$$\underline{\dot{\varepsilon}^{vp}} = \frac{3}{2}\dot{\gamma}\frac{dev\underline{\underline{\sigma}}}{\bar{\sigma}} - \frac{1}{3}\frac{\dot{\rho}}{\rho}\underline{I}, \tag{10}$$

where $\underline{I}$ is the second order identity tensor.

### 2.3 *The second principle of thermodynamics*

It can be reduced to the well-known Clausius-Duhem inequality, which can be split into the terms of intrinsic dissipation (the mechanical one) and the thermal dissipation. Assuming the classical hypotheses which comply with the thermal inequality, one can write the intrinsic term as follows [6] :

$$\underline{\sigma}\dot{\varepsilon}^{vp} - \rho\frac{\partial\Phi}{\partial z}\dot{z} \geq 0. \tag{11}$$

Dividing (11) by $\rho$, and using eq. (2) and (10), one obtains :

$$\frac{1}{\rho}\left[\frac{1}{K(\gamma)^{1/M}}\right]^{N}\bar{\sigma}^{N+1} + \pi^{f}\dot{z} \geq 0, \tag{12}$$

where $\pi^{f} = -\Phi^{*}(\varepsilon^{vp}, T) + F(1-2z) + \frac{1}{\rho_0}\frac{1-z_0}{(1-z)^2}\sigma_m$, and $\sigma_m = \frac{1}{3}tr(\underline{\sigma})$.

### *2.4 System evolution and kinetics*

One must now write a kinetic equation for z. This equation has to be consistent with the physics of the phenomena, and must also be consistent with equation (12).

From the definition of z, one can easily derive that $\frac{\dot{V}_f}{V_f} = \frac{\dot{z}}{z(1-z)}$, where $\dot{V}_f$ is the volume variation corresponding to the variation of z.

Hence, let us assume

- that there exist a threshold value (zero) for the thermodynamic force $\pi^{f}$ that allows the densification and swelling mechanisms (hence the porosity evolution),
- that $\frac{\dot{V}_f}{V_f} = G(\underline{\sigma}, T, BU)$ can be experimentally defined.

One can thus write

$$\dot{z} = H(\Omega)[z(1-z)G], \tag{13}$$

where $\Omega = G\pi^{f}$. H(x) is the Heavyside function.

This means that gas swelling ($\dot{z} < 0$) cannot proceed while $\pi^{f} \leq 0$ , and densification ($\dot{z} > 0$ ) occurs only when $\pi^{f} \geq 0$. The existence of a threshold value for densification and swelling is confirmed by some in pile experimental results.

Note also that the model complies automatically with the second law of thermodynamics thanks to the way the constitutive equations have been written.

## 3. SIMULATIONS AND DISCUSSIONS

### *3.1 The functions F and G*

The functions $F$ and $G$ play an important role on the global behavior of the material. Indeed, $F$ is responsible for the threshold value for the evolution of the porosity. It is difficult, at present time, to determine experimentally its value. As an example, let us consider the case where $\sigma$=0 at the beginning of the fuel's life. Thus $\pi^{f}$ depends only on $F$ ($z$ is equal to $z_0$). Thus the

evolution of F induces the one of the thermodynamic force associated to $z$. While $\pi^f$ is not equal to zero, $\dot{z} = 0$. But as soon as $\pi^f$ reaches the zero value, the function $\Omega$ reaches also zero and $\dot{z}$ can exist, depending on the value of $G$. That is, $F$ is governing the model in terms of threshold value, while the densification and gas swelling case are governed by $G$.

Moreover, the function $G$ acts directly on the viscoplastic strain rate. It can be determined experimentally by measurements of the volume variation. Thus, one can obtain the dependence of $G$ on the stress field, the temperature and the burnup. This determination is at present time performed by the CEA (Grenoble, France) in the frame of a cooperation between french companies involved in the nuclear industry.

As an example, one can see on figures 1-2 the effect of this function $G$ on creep simulation tests performed on the material, in the case where gas swelling prevails on densification. Figure 1 shows the influence of the function $G$ ($G = ct/\sigma$) on the creep tests (strain vs time, at $\sigma$ = 240 Mpa). Several values of $ct$ are chosen. The corresponding evolution of z is given figure 2 . The influence of the porosity growth on the fuel non-linear mechanical properties is obvious, in particular for porosity above 10%, which is commonly reached at the pellet periphery zone.

### *3.2 The effect of irradiation*

#### *3.2.1 From the theoretical viewpoint*

Irradiation can be taken into account through different ways. The most natural one is to let $F$ and $G$ depend on the burnup. It is physically what happens because densification and gas swelling depend directly on it. The determination of $G$ by the CEA shall be consistent with this statement.

On the other hand, the irradiation affects not only the evolution of the porosity distribution inside the material, but also the "structural" viscoplastic behavior of the material. Indeed, the material mechanisms that are responsible for viscoplasticity, i.e., grain boundary slipping, creation and migration of dislocations, are altered by irradiation (i.e., fission products, restructuring, secondary compounds,...). Hence, it seems logical to let the parameters (K, M, N) of the deviatoric part of the strain rate depend on the burnup.

The introduction of the burnup in such constitutive equations does not present any difficulty, because the presented frame is open enough.

#### *3.2.2 From the experimental viewpoint*

All what has been presented above is valid whatever the material is irradiated or not. The identification of the constitutive parameters is quite easy on non-irradiated material, because specimens of good quality are available. The problem is not so simple for irradiated material, because it becomes fractured, and one cannot use any specimen to perform classical macroscopic tests. Thus, it has been decided to develop other experimental techniques to provide tests useful for the parameter identification.

To this aim, EDF and the Institute for Transuranium Elements of Karlsruhe (Germany) develop together a microindentation technique [3]. A device has been designed and built. It will allow to perform mechanical tests on small irradiated specimens. Rational curves $\sigma$,$\varepsilon$ (at

constant strain rate), creep and relaxation tests will thus help one to improve the constitutive equation relative to the deviatoric part of the strain rate. For instance, a kinematic hardening could be added, or one could take into account restauration effects.

Nevertheless, the experimental results available do not fully correspond to those obtained from classical mechanical tests. This is due to the fact that the stress state induced by the microindenter is highly non-homogeneous. Thus, it is necessary to develop an original identification method devoted to this type of tests. An inverse method coupled with a finite element calculation shall provide the solution desired.

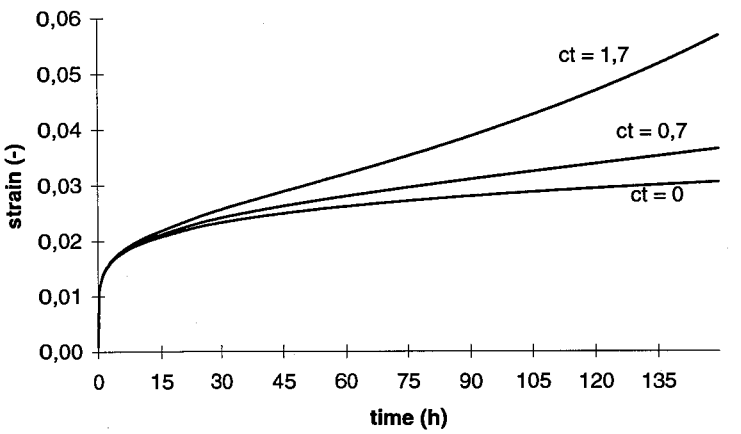


Fig.1 : Creep test

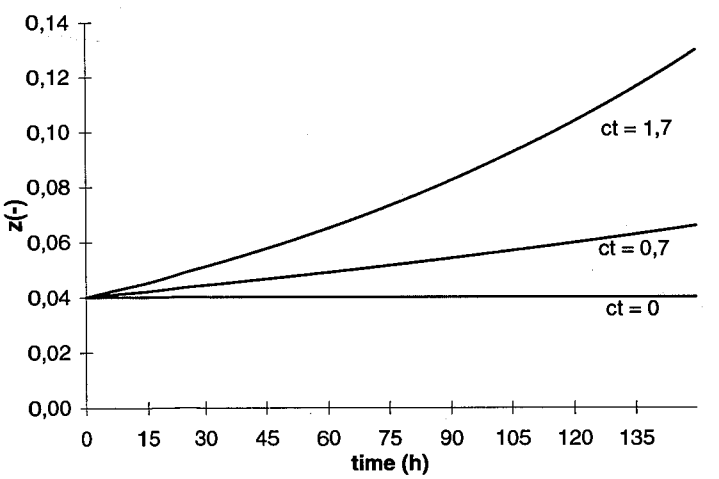


Fig.2 : Porosity evolution

## 4. CONCLUSIONS

The main objective of the present paper was to clearly exhibit the important role of the porosity on the fuel mechanical behavior. It has been shown that viscoplastic properties are activated by the evolution of the porosity. A general framework has been developed, in agreement with the principles of thermodynamics of irreversible processes. The major result of the present model concerns the fact that the viscoplastic strain is non-deviatoric, due to the porosity growth. The purely deviatoric part of the non-linear strain is taken as the Lemaître law, but any other classical equation may be used. As concerns the hydrostatic part, it is derived from simple assumptions. The coupling between the volume fraction of porosity and the mechanical stress field is introduced into the dissipation term.

The problem is now to clearly identify the functions $F$ and $G$, in order to establish how the porosity evolves with respect to the mechanic and physic conditions. Mechanical tests on irradiated material, in particular in the so-called rim zone, shall provide numerous informations in a near future. Thus, the next step will be to implement such a model into the existing numerical codes devoted to the fuel rod, in order to improve their capabilities as regards the mechanical simulation of the fuel pellet behavior.

## REFERENCES

1. Rice, J.R. 1971. Inelastic constitutive relations for solids : an internal-variable theory and its application to metal plasticity, *J. Mech. Phys. Solids*, **19**, 433-455.

2. Delobelle, P., Robinet, P., Geyer, P., Bouffioux, P., Le Pichon, I. 1995. A unified model to describe the anisotropic viscoplastic behavior of zircaloy-4 cladding tubes, *proc. 11th Symposium « zirconium in the nuclear industry », ASTM STP, Garmish-Partenkirchen.*

3. Baron, D., Leclercq, S., Spino, J., Taheri, S. 1996. Development of a microindentation technique to determining the fuel mechanical behaviour at high burnup, *IAEA Technical Commitee Meeting on Advances in Pellet Technology for improved Performance and High Burnup. Tokyo, 26 October-1 November.*

4. Leclercq, S., Lexcellent, C. 1996. A general macroscopic description of the thermomechanical behavior of shape memory alloys, *J. Mech. Phys. Solids*, **44**, 6, 953-980.

5. Olander, D.O. 1976. *Fundamental aspects of nuclear reactor fuel elements*, Technical Information Center, Office of Public Affairs, Energy Research and Development Administration, Berkeley.

6. Lemaître, J., Chaboche, J.L. 1985. *Mécanique des Matériaux Solides*, Dunod, Paris.

## ACKNOWLEDGEMENT

The author whish to thank Dr G. Rousselier for the scientific discussions that initiated this work, and D. Baron and J.M. Ruck for their fruitful remarks.

Transactions of the **14th International Conference on Structural Mechanics in Reactor Technology** (SMiRT 14), Lyon, France, August 17-22, 1997 **CW/6**

# A continuum model for the mechanical behaviour of UO2 fuel under cracking, relocation and PCMI

**Jernkvist L.O.**
*ABB Atom, Sweden*

ABSTRACT:

This paper presents a constitutive model for cracked and fragmented uranium dioxide fuel pellets in light water reactor fuel rods. The proposed model, in which cracks are represented by nonelastic strains in a continuum context, accounts for the fuel mechanical behaviour under pellet cracking, fragment relocation and pellet-clad mechanical interaction. Moreover, the detrimental effect of cracking on the fuel thermal conductivity is considered in the model.

## 1. BACKGROUND

When uranium dioxide fuel is taken into operation and brought up to power, the fuel pellets crack as soon as the thermally induced tensile stresses exceed the material fracture stress [1]. The cracks strongly influence both the thermal and the mechanical performance of the fuel [2].

Heat transfer is affected, since flow induced vibrations (FIV) and/or power cycling cause fuel fragments to move radially outward, closing the pellet-clad gap and opening internal gaps along the cracks. This process, which is referred to as pellet relocation, leads to an improved pellet-clad heat transfer, but also to an anisotropic degradation of the fuel thermal conductivity. Taken together, the result is a significantly altered temperature distribution in the cracked fuel.

Pellet-clad mechanical interaction (PCMI) is also affected by the cracking, since the cracked material exhibits an apparent stiffness, much lower than that of the uncracked virgin material. When the fuel is compressed, crack closure takes place under increasing resistance, and the fuel macroscopic stiffness gradually increases. Complete crack closure is generally not obtained, since geometric mismatch obstructs fragments from returning to their original positions [3].

Over the years, numerous models for the cracked fuel properties have been proposed. At the beginning, the thermal effects of cracking were of primary interest, because of their relevance to fission gas release and fuel stored energy. The pellet-clad gap reduction due to fuel fragment relocation was modelled by postulating a growing pellet radius with fuel power and burnup [4].

With the advent of PCI-induced fuel rod failures in the seventies, the focus shifted to constitutive modelling of the cracked fuel mechanical behaviour. Several damage-like models appeared, in which fuel cracking was treated in a two-dimensional context by reducing the elastic stiffness of the material [5-7]. The stiffness reduction results in an increase of the pellet radius, but in contrast to reality, the obtained relocation is fully reversible upon unloading. However, by treating cracking as nonelastic deformation, this shortcoming is alleviated [8].

The later approach has been the starting point for the model presented here, in which cracks are represented by nonelastic strains in a continuum context. The derived model has the form of a general non-linear stress-strain relation, with close resemblance to associated plasticity in strain-softening materials. The constitutive relation is suited for implementation in two- or three-dimensional finite element fuel rod analysis programs.

## 2. GENERAL FORMULATION OF THE MODEL

In the proposed model, fuel cracking is treated in a continuum context, where the influence of cracks on the thermal and mechanical properties is averaged or 'smeared' over a finite material volume. As a consequence, the material is assumed to posses a gradually decreasing load bearing capacity as cracks nucleate. Under uniaxial tension, the material is assumed to respond as illustrated in the upper part of figure 1. The response under compression is depicted in the lower part of the figure. Crack closure takes place under increasing resistance, since the irregular crack surfaces obstruct the fragments return to their original positions.

The material behaviour in figure 1 may be described by a stress-strain relation in the form

$$\sigma = E(\varepsilon - \varepsilon_c) \tag{1}$$

where $\sigma$ is the Cauchy stress, $E$ is Young's modulus, $\varepsilon$ is the total strain and $\varepsilon_c$ is the crack strain. $\varepsilon_c$ is a function of the applied load history, such that the behaviour in figure 1 is reproduced. The shaded area represents admissible stress states, for which the material exhibits a fully elastic behaviour. The boundaries of the area are defined by two functions; one representing fuel cracking and the other fragment compression.

The outlined uniaxial behaviour is generalised to a three-dimensional stress state by analogy with the route taken in the theory of associated plasticity: First, the constitutive relation (1) is rewritten in the form of Hooke's generalized law. Secondly, an envelope to all admissible stress states in a multidimensional stress space is defined. The resulting hypersurface corresponds to the yield surface in plasticity. Finally, an evolution law for the crack strain is formulated, such that any non-admissible stress state can be brought to an admissible state through the constitutive relation. This evolution law corresponds to the flow rule in plasticity. The above three steps are described in detail in the following subsections.

### *2.1 The constitutive relation*

The applied stress-strain relation is Hooke's law, written in terms of stress and strain rates:

$$\dot{\boldsymbol{\sigma}} = \boldsymbol{D}:(\dot{\boldsymbol{\varepsilon}} - \dot{\boldsymbol{\varepsilon}}_c) \tag{2}$$

Here, $\dot{\boldsymbol{\sigma}}$ is the Cauchy stress rate tensor, $\boldsymbol{D}$ is the material stiffness tensor, $\dot{\boldsymbol{\varepsilon}}$ is the total linear strain rate tensor, $\dot{\boldsymbol{\varepsilon}}_c$ is the crack strain rate, and colon denotes a contracted tensor product. The restriction to linear strains and Cauchy stress rates is justified, since the expected deformations and rotations are small. In equation (2), nonelastic strains from fuel thermal expansion, swelling, densification and creep have been omitted for simplicity.

### *2.2 Admissible stress states*

The admissible stress states, which define the region of elastic behaviour, are discerned by means of the following three fundamental postulates:

1) The maximum principal stress is limited by the materials fracture stress (Rankines criterion). When cracking proceeds, the load bearing capacity of the material progressively decreases.

2) Crack closure will take place under a sufficient compressive stress normal to the crack. The compressive stress needed for crack closure decreases with temperature.

3) Only a limited shear stress can be sustained across a crack without causing slip of adjacent crack surfaces. This critical stress drops gradually as the crack opens.

The above postulates can be cast into analytical form by considering the principal stress space and the principal directions of crack strain. With reference to figure 2, let the principal directions of the crack strain tensor be $\boldsymbol{c}_1$, $\boldsymbol{c}_2$ and $\boldsymbol{c}_3$, corresponding to the principal crack strains ${}_1\varepsilon_c > {}_2\varepsilon_c > {}_3\varepsilon_c \geq 0$. Since we in general have more than one of the principal crack strains greater than zero, the crack in figure 2 should be interpreted rather as a band, comprising a number of variously oriented cracks. $\boldsymbol{c}_1$ then defines the most probable crack surface normal among these cracks. In the same manner, let $\boldsymbol{s}_1$, $\boldsymbol{s}_2$ and $\boldsymbol{s}_3$ define the principal directions of the stress tensor, and ${}_1\sigma > {}_2\sigma > {}_3\sigma$ be the corresponding principal stresses.

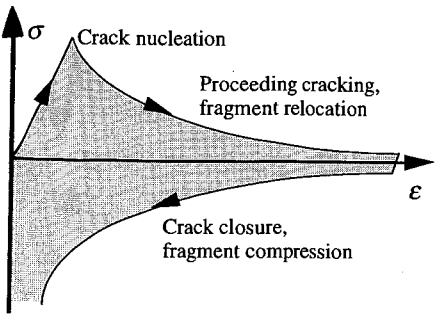


*Fig 1. Stress-strain relation for the cracked material under uniaxial deformation.*

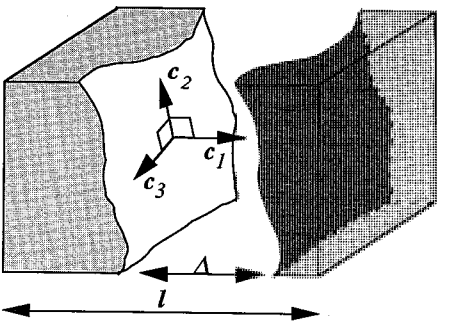


*Fig 2. Interpretation of the principal axes of the crack strain tensor.*

The principal stresses and strains may be expressed as

$$ {}_i\sigma = \boldsymbol{S}_{ii}:\boldsymbol{\sigma} \tag{3} $$

$$ {}_i\varepsilon_c = \boldsymbol{C}_{ii}:\boldsymbol{\varepsilon}_c \tag{4} $$

where the projection operators $\boldsymbol{S}$ and $\boldsymbol{C}$ in equations (3) and (4) are given by

$$ \boldsymbol{S}_{ij} = \frac{1}{2}\left( \boldsymbol{s}_i \otimes \boldsymbol{s}_j + \boldsymbol{s}_j \otimes \boldsymbol{s}_i \right) \tag{5} $$

$$ \boldsymbol{C}_{ij} = \frac{1}{2}\left( \boldsymbol{c}_i \otimes \boldsymbol{c}_j + \boldsymbol{c}_j \otimes \boldsymbol{c}_i \right) \tag{6} $$

With this notation, the three fundamental postulates may be formulated as inequalities:

$$ F_1 = \boldsymbol{S}_{11}:\boldsymbol{\sigma} - \sigma_f(\boldsymbol{S}_{11}:\boldsymbol{\varepsilon}_c) \leq 0 \qquad \text{( Crack nucleation and growth )} \tag{7} $$

$$ F_2 = \sigma_c(\boldsymbol{C}_{11}:\boldsymbol{\varepsilon}_c) - \boldsymbol{C}_{11}:\boldsymbol{\sigma} \leq 0 \qquad \text{( Crack closure under compression )} \tag{8} $$

$$ F_3 = \boldsymbol{C}_{12}:\boldsymbol{\sigma} - \sigma_s(\boldsymbol{C}_{11}:\boldsymbol{\varepsilon}_c) \leq 0 \qquad \text{( Crack surface slip under shear )} \tag{9a} $$

$$ F_4 = -\boldsymbol{C}_{12}:\boldsymbol{\sigma} - \sigma_s(\boldsymbol{C}_{11}:\boldsymbol{\varepsilon}_c) \leq 0 \qquad \text{( - " - )} \tag{9b} $$

$$ F_5 = \boldsymbol{C}_{13}:\boldsymbol{\sigma} - \sigma_s(\boldsymbol{C}_{11}:\boldsymbol{\varepsilon}_c) \leq 0 \qquad \text{( - " - )} \tag{9c} $$

$$ F_6 = -\boldsymbol{C}_{13}:\boldsymbol{\sigma} - \sigma_s(\boldsymbol{C}_{11}:\boldsymbol{\varepsilon}_c) \leq 0 \qquad \text{( - " - )} \tag{9d} $$

Here, $\sigma_f$ is the material fracture stress, $\sigma_c$ is the stress needed for crack closure and $\sigma_s$ is the shear stress that can be sustained across a crack band. These are all functions of the material crack density, and will be further discussed in section 4.

### 2.3 *Crack evolution law*

Whereas the definition of admissible stress states is rather straightforward, the definition of a crack evolution law is more indefinite. Since the information deduced from experiments and material testing is limited, evolution laws are generally based on theoretical models, to which general principles of thermodynamics set restrictions. A convenient approach is provided by the theory of associated plasticity, in which the principle of maximum dissipation leads directly to an evolution law, once the yield surface is defined. This theory has strong experimental support for plastic deformation in metals, and its applicability to crack formation in brittle non-metallic materials has recently been demonstrated [9-10].

Following the concept of associated plasticity in materials with multiple yield surfaces [11] we may write the crack strain rate as

$$\dot{\boldsymbol{\varepsilon}}_c \;=\; \sum_{i=1}^{6} \frac{\partial F_i}{\partial \boldsymbol{\sigma}} \dot{\lambda}_i \tag{10}$$

where $F_i$ are the conditions on admissible stress states defined in equations (7)-(9) and $\dot{\lambda}_i$ are scalar parameters. $\dot{\lambda}_i$ define the effective strain rate related to cracking, crack closure and crack surface slip, and have to comply with the Kuhn-Tucker conditions:

$$\dot{\lambda}_i \;\geq\; 0, \qquad F_i \;\leq\; 0, \qquad \dot{\lambda}_i F_i \;=\; 0 \tag{11}$$

Equations (7) to (10) result in a final expression for the crack strain evolution law:

$$\dot{\boldsymbol{\varepsilon}}_c \;=\; \boldsymbol{S}_{11}\dot{\lambda}_1 - \boldsymbol{C}_{11}\dot{\lambda}_2 + \boldsymbol{C}_{12}\left(\dot{\lambda}_3 - \dot{\lambda}_4\right) + \boldsymbol{C}_{13}\left(\dot{\lambda}_5 - \dot{\lambda}_6\right) \tag{12}$$

Equation (12) is a general formulation of the crack evolution law for a 3-D geometry. The projection operators $\boldsymbol{S}_{ij}$ and $\boldsymbol{C}_{ij}$ are given by the eigenvectors of the current stress and crack strain tensors through equations (5) and (6). The parameters $\dot{\lambda}_i$ so far remain undetermined, but will be further discussed in section 4.

## 3. THERMAL CONDUCTIVITY DEGRADATION DUE TO CRACKS

The nascence of cracks impairs heat transfer in the fuel material, and the extent of impairment is dictated by the density, location and orientation of the cracks. Circumferential cracks created by radial tensile stresses under ramp down are particularly detrimental, since they are perpendicular to the main heat flow. Let us assume that the heat flow in both the uncracked and cracked material can be described by Fourier's law for heat conduction

$$\boldsymbol{j} \;=\; -\boldsymbol{k} \cdot \nabla T \tag{13}$$

where $\boldsymbol{j}$ is the heat flux vector, $\boldsymbol{k}$ the thermal conductivity tensor and $\nabla T$ the temperature gradient. Since the original uncracked material is isotropic, the components of $\boldsymbol{k}$ are

$$k_{ij} \;=\; k_o \delta_{ij} \tag{14}$$

where $k_o$ is the thermal conductivity of the uncracked material and $\delta_{ij}$ is Kroenecker's delta. This simple form of $\boldsymbol{k}$ will be lost at onset of cracking, since the opening of cracks leads to anisotropic degradation of the thermal conductivity. This degradation is easily modelled, if we assume the principal axes of $\boldsymbol{k}$ always to be aligned with the principal axes of crack strain; $\boldsymbol{c}_1$, $\boldsymbol{c}_2$ and $\boldsymbol{c}_3$. The conductivity tensor may then be written in a spectrally decomposed form:

$$\boldsymbol{k} \;=\; {}_1k\,\boldsymbol{C}_{11} + {}_2k\,\boldsymbol{C}_{22} + {}_3k\,\boldsymbol{C}_{33} \tag{15}$$

where ${}_ik$ is the principal value of $\boldsymbol{k}$, associated with the principal axis $\boldsymbol{c}_i$. ${}_ik$ is a decreasing function of ${}_i\varepsilon_c$, which is the principal crack strain in the $\boldsymbol{c}_i$-direction.

The relation between ${}_ik$ and ${}_i\varepsilon_c$ may be deduced by considering the one-dimensional geometry in figure 2. Assuming a heat flux $j$ across the crack, the temperature drop $\Delta T$ over the slab is

$$\Delta T = j\left(\frac{l-\Delta}{k_o}\right)+\Delta T_c \tag{16}$$

where $l$ is the original length of the slab, $\Delta$ is the crack opening and $\Delta T_c$ is the temperature jump across the crack. If gas conductance is the only mode of heat transfer across the crack, $\Delta T_c$ can be calculated from

$$\Delta T_c = \frac{j}{k_g}\left(\Delta + e_a + e_b\right) \tag{17}$$

where $k_g$ is the thermal conductivity of the gas in the crack and $e_a$, $e_b$ denote the extrapolation lengths (jump distances) at the crack surfaces a and b. The gas thermal conductivity $k_g$ depends strongly on the gas composition and temperature. From (16) and (17) the effective thermal conductivity in the $\boldsymbol{c}_1$-direction of the cracked material is found to be

$${}_1k = \frac{jl}{\Delta T} = k_o\left(1+\frac{k_o}{k_g}\left(\frac{e_a+e_b}{l}\right)+\frac{\Delta}{l}\left(\frac{k_o}{k_g}-1\right)\right)^{-1} \tag{18}$$

Identifying $\Delta/l$ as the principal crack strain in the $\boldsymbol{c}_1$-direction, ${}_1\varepsilon_c$, and introducing

$$\beta = \frac{k_o}{k_g}\left(\frac{e_a+e_b}{l}\right) \tag{19}$$

we have the following expression for the degraded thermal conductivity

$${}_1k = k_o\left(1+\beta+{}_1\varepsilon_c\left(\frac{k_o}{k_g}-1\right)\right)^{-1} \tag{20}$$

The parameter $\beta$ in equation (19) is found to be roughly 0.01, fairly independent of the composition and temperature of the gas. The parameter $l$ represents the average spacing between adjacent cracks, which is in the order of 1 mm. The extrapolation lengths are dependent on the gas and crack surface properties, but are generally less than 1 μm. Recognising that $\beta << 1$ and ${}_1\varepsilon_c << 1$, equation (20) can be further simplified:

$${}_ik = k_o\left(1+\frac{k_o}{k_g}{}_i\varepsilon_c\right)^{-1} \qquad \frac{k_o}{k_g} >> 1 \tag{21}$$

According to equation (21), the conductivity degradation is dependent on the gas composition. The influence of cracking on fuel thermal conductivity thus exacerbates at high burnup, when gaseous fission products with low thermal conductivity are accumulated in fuel internal cracks.

## 4. NUMERICAL IMPLEMENTATION OF THE MODEL

### *4.1 Fracture- and closure stress correlations*

For implementation of the proposed model in a fuel performance computer code, the general expressions in section 2 need be complemented with correlations for the fracture- and closure stress in equations (7)-(9). In the sequel, expressions are given for these quantities, that have been derived from analytical solutions and experimental observations on fuel cracking and fragment compression.

The tensile stress that can be sustained across a given crack band is assumed to drop exponentially with the crack strain normal to the crack, $\varepsilon_c$

$$\sigma_f(\varepsilon_c) = \sigma_f^o e^{-\alpha \varepsilon_c} \tag{22}$$

The same relationship is also used for the critical shear stress across the crack, $\sigma_s$

$$\sigma_s(\varepsilon_c) = \sigma_f^o e^{-\alpha \varepsilon_c} \tag{23}$$

where $\sigma_f^o$ is the fracture stress of the uncracked material and $\alpha$ is a positive constant, which is correlated to the energy dissipation per unit volume under cracking. $\sigma_f^o$ depends mainly on fuel temperature, grain size and porosity [12]. The compressive stress needed for crack closure is calculated through

$$\sigma_c(\varepsilon_c) = a\left( \frac{b}{\varepsilon_c} \right)^n \tag{24}$$

where $\varepsilon_c$ is the crack strain normal to the crack, $b$ is a constant and the parameters $a$ and $n$ are decreasing functions of temperature.

### *4.2 Localised cracking and viscous regularization*

In the proposed continuum crack model, formation of cracks is manifested as anisotropic material softening. This softening causes numerical difficulties, since it leads to a localization of crack strains into the point at which cracking first appears, and thereby also to a highly discontinuous solution. For this reason, the solution will exhibit a severe dependence on the spatial discretization, unless a characteristic length scale is introduced in the problem, eg by use of a non-local continuum model, a gradient dependent flow rule, or viscous regularization [13].

The technique of viscous regularization, in which a fictitious viscosity is introduced in the constitutive relation, is numerically the most tractable approach, since it allows integration of the constitutive relation locally. When strain softening occurs at a certain point, the viscous behaviour will prevent immediate localization of deformation into that point. Instead, the load will redistribute to the neighbourhood and the deformation is propagated over a larger region. Viscous regularization is used in our implementation, which is presented in section 5. The crack strain rates $\dot{\lambda}_i$ in equation (10) are then calculated through

$$\dot{\lambda}_i = \frac{\gamma}{\mu_i}\left( \frac{\langle F_i \rangle}{\gamma} \right)^{m_i} \tag{25}$$

where $\gamma$ and $m_i$ are model parameters, $\mu_i$ are viscosities related to cracking, crack closure and crack surface slip, and the Macauley brackets are defined by

$$\langle F_i \rangle = \frac{1}{2}\left( F_i + |F_i| \right) \tag{26}$$

By use of equation (25), it can be seen that the conditions in (11) are incontestably satisfied.

The viscosities for cracking and crack surface slip serve solely for regularizing the strain-softening problem, and have no physical interpretation. Crack closure is on the other hand a time dependent process, and the corresponding viscosity thus has a physical significance. The closure rate is believed to be governed by flow induced vibrations at low temperature, whereas creep and grain growth are the rate controlling processes at high temperature [14]. At high temperature, crack closure may ultimately result in crack healing, provided that the material is held in compression for a sufficient length of time. The crack surfaces are then sintered together, and the original material properties are more or less recovered [15].

## 5. EXAMPLE APPLICATIONS

In this section, the models ability to capture various aspects of the cracked fuel behaviour is demonstrated by comparing model predictions with experimental results. The cracked fuel constitutive model was implemented in the ABB Atom STAV-T fuel performance program, which is a two-dimensional finite element code intended for transient thermal and mechanical analyses of light water reactor fuel rods [16]. The implementation was performed by substituting the existing plastic flow rule with the presented model for the cracked fuel material.

### *5.1 Crack nucleation*

The number of radial cracks intersecting the pellet surface was correlated to linear heat generation rate (LHGR) in a post irradiation examination [3], where 45 fuel rods were inspected. The measured number of radial cracks was compared with the calculated hoop crack strain at the pellet periphery. The comparison was made with respect to maximum LHGR experienced under operation. The result is shown in figure 3. It is seen that the onset of cracking at a LHGR of 5 $kWm^{-1}$ is captured by the model, as well as the saturation in cracking for heat rates above 30 $kWm^{-1}$, when nucleation of cracks is counterbalanced by crack healing and creep relaxation.

### *5.2 Fragment ratcheting*

The effect of power cycling on fuel relocation was experimentally studied in [17], where a large gap fuel rod was held at a constant LHGR of 27 $kWm^{-1}$, up to a burnup of 2.6 MWd/kgU. Under this period, 5 reactor shutdowns were carried out. At each shutdown, the pellet-clad gap was determined by fuel centreline measurements just before and just after shutdown, and the reduction in gap size between these two measurements was ascribed to fragment ratcheting. Figure 4 shows the calculated radial displacement of the pellet surface as a function of time, and table 1 gives the measured and predicted radial gap size reduction at shutdown 1 to 5.

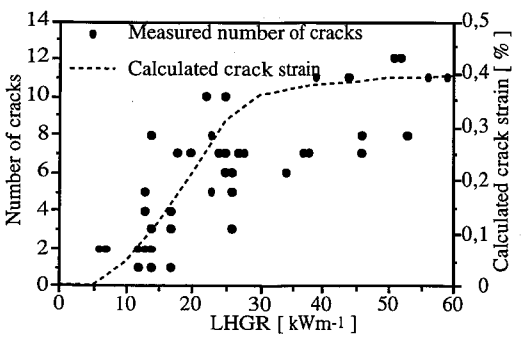


*Fig 3. Number of observed cracks and calculated crack strain vs LHGR.*

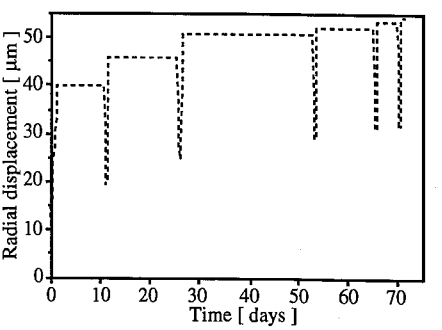


*Fig 4. Calculated radial displacement of the pellet surface.*

*Tab 1. Fuel fragment ratcheting at successive shutdowns*

| Shutdown: | Time: [days] | Burnup: [MWd/kgU] | Fragment ratcheting [µm]: Measured | Predicted |
|---|---|---|---|---|
| 1 | 11.4 | 0.36 | 8.4 | 6.1 |
| 2 | 26.1 | 0.83 | 6.8 | 4.7 |
| 3 | 53.3 | 1.70 | 1.3 | 1.6 |
| 4 | 65.6 | 2.09 | 0.6 | 1.2 |
| 5 | 70.5 | 2.25 | 0.5 | 0.7 |

## 6. CONCLUSIONS

A continuum model for the cracking and post-cracking behaviour of $UO_2$ fuel was presented. The model is derived in the form of a non-linear constitutive relation, that may easily be implemented in any two- or three-dimensional finite element computer code with capability to treat material non-linearities. A procedure for evaluating the detrimental effects of cracks on fuel thermal conductivity was also proposed. Comparisons with experimental investigations confirm that several phenomena related to the in-reactor behaviour of $UO_2$ fuel are captured by the model. The nucleation of cracks at a certain critical heat generation rate, fuel fragment radial relocation, crack healing and ratcheting of fuel fragments are satisfactory represented.

## 7. REFERENCES


[1] M. Oguma, 1983. Cracking and relocation behaviour of nuclear fuel pellets during rise to power, *Nucl. Eng. Des.* 76: 35-45.

[2] E. Kolstad et al, 1983. Review of test results on gap closure behaviour and mechanical interaction effects in HBWR, *OECD Halden Reactor Project Report* HWR 89.

[3] L.A. Walton and D.L. Husser, 1983. Fuel pellet fracture and relocation, *Proc. of the IAEA specialist's meeting on water reactor fuel element performance computer modelling*, Preston, UK, Applied Science Publishers, 1983, 115-135.

[4] K. Lassmann and H. Blank, 1988. Modelling of fuel rod behaviour and recent advances of the TRANSURANUS code, *Nucl. Eng. Des.* 106: 291-313.

[5] H.J. Ritzhaupt-Kleissl and M. Heck, 1993. SATURN-FS1, a computer code for thermo-mechanical fuel rod analysis, *Kernforschungszentrum Karlsruhe Report* KFK 5203.

[6] T. Nakajima, H. Saito, T. Ousaka, 1988. Fuel behavior code FEMAXI-IV and its application, *IAEA technical committee meeting on water reactor fuel element computer modelling in steady state, transient and accident conditions*, Preston UK, September 19 - 22, 1988.

[7] Y.R. Rashid, R.S. Dunham and Y.M. Lu, 1983. FREY-01: Fuel rod evaluation system, Volume 1: Theoretical and numerical bases, *EPRI Report* EPRI NP-3277-CCM, Project 1321-4.

[8] K. Lassmann, 1977. An iterative model for calculating the crack structure in fuel rod design, *Trans. 4th Int. Conf. on Structural Mechanics in Reactor Technology*, 1977, Vol C, paper C 1/3.

[9] S. Govindjee, G.J. Kay, J.C. Simo, 1995. Anisotropic modelling and numerical simulation of brittle damage in concrete, *Int. J. Num. Met. Eng.* 38: 3611-3633.

[10] P.H. Feenstra, R. De Borst, 1995. A plasticity model and algorithm for mode I-cracking in concrete, *Int. J. Num. Met. Eng.* 38: 2509-2529.

[11] W.T. Koiter, 1953. Stress-strain relations, uniqueness and variational theorems for elastic-plastic materials with singular yield surface, *Quarterly Applied Mathematics* 11: 350-354.

[12] R.F. Canon, J.T.A. Roberts, R.J. Beals, 1979. Deformation of $UO_2$ at high temperatures, *J. American Ceramic Society* Vol 54, No 2, 105-112.

[13] Z.P. Bazant and L. Cedolin, 1991. *Stability of structures; Elastic, inelastic, fracture and damage theories*, Oxford University Press, ISBN 0-19-505529-2.

[14] R.E. Williford and D.D. Lanning, Cracked fuel mechanics, 1983. *Proc. of the IAEA specialist's meeting on water reactor fuel element performance computer modelling*, Preston, UK, Applied Science Publishers, 1983, 153 - 186.

[15] J.B. Ainscough, F. Rigby, 1973. Measurements of crack sintering rates in $UO_2$ pellets. *J. Nucl. Mat.* 47: 246-250.

[16] A.R. Massih, T. Rajala, L.O. Jernkvist, 1995. Analyses of pellet-cladding mechanical interaction behaviour of different ABB Atom fuel rod designs, *Nucl. Eng. Des.* 156: 383-391.

[17] J.B. Ainscough, C. Lang, D.A. Moore, D.J. Clough, 1980. In-reactor densification and relocation of $UO_2$ fuel, *Proc. IAEA specialist's meeting on water reactor fuel element performance computer modelling* Blackpool, UK, 17-21 March, 1980.